Article

Identifying Key Drivers of Efficient B Cell Responses: On the Role of T Help, Antigen-Organization, and Toll-like Receptor Stimulation for Generating a Neutralizing Anti-Dengue Virus Response

Jan M. Sobczak [1,2,*,†], Irena Barkovska [3,†], Ina Balke [3], Dominik A. Rothen [1,2], Mona O. Mohsen [1,2], Dace Skrastina [3], Anete Ogrina [3], Byron Martina [4,5], Juris Jansons [3], Janis Bogans [3], Monique Vogel [1,2], Martin F. Bachmann [1,2,6,‡] and Andris Zeltins [3,‡]

[1] Department of Immunology, University Clinic of Rheumatology and Immunology, Inselspital, CH-3010 Bern, Switzerland; dominik.rothen@unibe.ch (D.A.R.); mona.mohsen@unibe.ch (M.O.M.); monique.vogel@unibe.ch (M.V.); martin.bachmann@me.com (M.F.B.)
[2] Department of BioMedical Research, University of Bern, CH-3008 Bern, Switzerland
[3] Latvian Biomedical Research and Study Centre, LV-1067 Riga, Latvia; irenabarkovska@gmail.com (I.B.); inab@biomed.lu.lv (I.B.); dace.skrastina@biomed.lu.lv (D.S.); anete.ogrina@biomed.lu.lv (A.O.); jansons@biomed.lu.lv (J.J.); janis.bogans@gmail.com (J.B.); anze@biomed.lu.lv (A.Z.)
[4] Artemis Bioservices, 2629 JD Delft, The Netherlands; b.martina@artemisbioservices.com
[5] Protinhi Therapeutics, 6534 AT Nijmegen, The Netherlands
[6] Nuffield Department of Medicine, The Jenner Institute, University of Oxford, Oxford OX3 7BN, UK
* Correspondence: jan.sobczak@unibe.ch
† These authors contributed equally to this work.
‡ These authors contributed equally to this work.

Abstract: T help (Th), stimulation of toll-like receptors (pathogen-associated molecular patterns, PAMPs), and antigen organization and repetitiveness (pathogen-associated structural patterns, PASPs) were shown numerous times to be important in driving B-cell and antibody responses. In this study, we dissected the individual contributions of these parameters using newly developed "Immune-tag" technology. As model antigens, we used eGFP and the third domain of the dengue virus 1 envelope protein (DV1 EDIII), the major target of virus-neutralizing antibodies. The respective proteins were expressed alone or genetically fused to the N-terminal fragment of the cucumber mosaic virus (CMV) capsid protein—nCMV, rendering the antigens oligomeric. In a step-by-step manner, RNA was attached as a PAMP, and/or a universal Th-cell epitope was genetically added for additional Th. Finally, a PASP was added to the constructs by displaying the antigens highly organized and repetitively on the surface of CMV-derived virus-like particles (CuMV VLPs). Sera from immunized mice demonstrated that each component contributed stepwise to the immunogenicity of both proteins. All components combined in the CuMV VLP platform induced by far the highest antibody responses. In addition, the DV1 EDIII induced high levels of DENV-1-neutralizing antibodies only if displayed on VLPs. Thus, combining multiple cues typically associated with viruses results in optimal antibody responses.

1. Introduction

The comprehensive goal for any vaccine candidate is to induce strong and long-lasting antibody (Ab) responses. This can be achieved by displaying the epitopes of interest in a maximally immunogenic manner [1–3]. One of the most effective strategies for designing both protective and safe new-generation vaccines involves mimicking the characteristic traits of pathogens, including their size, shape, and surface molecular organization, whilst excluding their infectivity [2,3]. Thus, viral mimetics, such as virus-like particles (VLPs),

serve as effective and well-established platforms to endow selected antigens with a viral appearance. VLPs are nanostructures composed of spontaneously assembling proteins that form spherical, rod-shaped, or filamentous particles [4–6]. Continuously developed over the past four decades [4,7–10], VLP-based vaccines have evolved from targeting their source viruses [7,8,11–25] to incorporating epitopes from various pathogens, including viruses [26–31], bacteria [32,33], and parasites [34–38]. Moreover, they have also been used to address chronic and non-communicable diseases [39–48].

Due to their universal properties, antigen-fused VLPs have attracted significant interest as vaccine vectors, offering a broad spectrum of potential applications [49–52]. However, fusing an antigen to the viral capsid or coat proteins (CPs)—building blocks of VLPs— may result in undesirable outcomes such as the formation of insoluble inclusion bodies (IBs) [53], alterations in the shape of folded VLPs [5], or even ablated expression. These issues may arise due to the molecular weight of the antigen, its charge, or other sequence peculiarities, including repeats, pseudo-termination sequences, or rare tRNA codons. To address these, various strategies have been developed, including the expression of mosaic VLPs [54–59], or the binding of antigens by chemical [39,60–65], enzymatic [57,66–69], or physical [70–73] methods.

Beyond the whole viral CPs [50,51,74–77], the structural elements of CPs, such as the β-annulus peptide [78–80], or other genetically encoded proteins capable of self-assembling into multimeric nanostructures, are also potentially applicable in vaccine development. These include ferritin [74,81–85], encapsulin [74,84,86–89], lumazine synthase [74,84,90–92], transferrin [85,93–95], lactoferrin [85,96], casein [85,97–99], non-viral pyruvate dehydrogenase E2 protein [100–102], GCN4-based isoleucine zipper [103–105], the T4 bacteriophage fibritin foldon [104,106,107], WA20-foldon (a complex of WA20 protein and T4 bacteriophage fibritin) [108,109], or magnetosomes [85,110–112].

Nanostructures, to be used as vaccine platforms, must be able to induce a significant immune response against displayed antigens. Their design should ideally generate robust B- and T-cell responses, including long-lived plasma cells secreting high-affinity Abs [113]. To achieve such favorable immune responses, the dynamics of antigen exposure and innate stimulation must be optimally designed. This can be obtained by modifying both the exterior and interior surfaces of nanostructures, or VLPs [114]. It involves the incorporation of pathogen-associated molecular patterns (PAMPs)—the molecular signatures derived from pathogens and recognized by the immune system—and pathogen-associated structural patterns (PASPs), referring to the spatial arrangement of antigens characteristic of pathogen surfaces [1–3]. PASPs are recognized by natural Abs and the complement system, which enhances the uptake of a nanostructure/VLP by an antigen-presenting cell (APC), thereby facilitating T-cell priming [115]. A classic study by Vogelstein and colleagues identified an optimal antigen density on nanoparticles for PASP, which maximizes B-cell activation, to be within the 5–10 nm range [116].

In contrast to PASPs, toll-like receptor (TLR)-stimulating PAMP elements included in the interior facets might be as effective as such modifications to the exterior [55,56,59]. The enhancement of immune response was previously demonstrated through the packaging of ssRNA, dsRNA, and CpGs [117–120], serving as ligands for TLR 7/8, TLR3, and TLR9, respectively [121–124]. Stimulation of TLR7, for instance, preferentially boosts the production of IgG2a/c and IgG2b subclasses in mice [87,91,125,126], which are crucial for protection against viral [92,127], bacterial [90,128], and parasite infections [93,129].

To enhance Th-cell-dependent B-cell responses, incorporating a strong, universal T-cell epitope can be beneficial [43,59,94]. These can be integrated into the structure of VLP/nanoparticle [43,130], but they are also used as short linear peptides [131,132], fused to proteins [133], coupled to carbohydrates [134], or co-assembled with self-assembling peptide nanofiber systems [135]. Examples of such universal epitopes include a Th-cell epitope from tetanus toxin (TT) [96,136–138], the transmembrane domain of the West Nile virus E protein [98,130], the adenovirus Ad5 E1a protein [139], or the synthetic, non-natural Pan DR Epitope (PADRE) [131,140,141].

PADRE is an engineered peptide known for its broad reactivity. It is capable of binding with high or medium affinity to 15 out of the 16 most common human HLA-DR haplotypes [131,141], as well as cross-reacting with mouse class II alleles [140,142]. Thus, PADRE, as a "universal" helper T-cell epitope, has been recognized for its effectiveness in enhancing CD4+ T-cell responses [131,140,141]. Like other T-cell epitopes, it has been utilized as a fusion peptide [131,143–151], a carbohydrate carrier [152,153], an adjuvant [143,154,155], and has been incorporated into liposomal formulations [156] or self-assembling nanofibers [157–159]. PADRE has been shown to be particularly useful in development vaccine candidates that induce desired self-responses in the context of non-communicable diseases [147,149,154–156,158,159], as demonstrated in several pre-clinical trials across various animal models, such as rat arthritis [147] or colorectal cancer [149]. However, its application also extends to the development of distinct protein-based anti-pathogenic vaccines [143–146,148,150,151,157], including those for *Toxoplasma gondii* [148,150], *Staphylococcus aureus* [157], SARS-CoV-2 [151], or DENV-2 [144]. This demonstrates the versatility of PADRE and suggests the potential benefits of including it in one of the vaccine platforms presented here.

Our research on cucumber mosaic virus (CMV)-derived VLPs, termed "CuMV" in our papers to avoid confusion with cytomegalovirus (which, like cucumber mosaic virus, is abbreviated CMV according to the ICTV classification), demonstrated the spontaneous encapsulation of prokaryotic ssRNA within the particles, which positively correlates with the formation of a high-avidity IgG response [160]. The encapsulation occurs during self-assembly in the bacterial system [55,56,59], a phenomenon consistent with findings regarding Qβ-derived VLPs [161]. Immunological optimization of CuMV VLPs was further carried out by incorporating into their interior facets a universal Th-cell epitope derived from TT (thus forming CuMV$_{TT}$ particles), leading to the development of multiple vaccine candidates that induce highly specific, class-switched neutralizing Abs [43,46,54–56,59,60,62,63,65,162–164]. However, the limited capacity for antigen fusion in CuMV$_{TT}$ VLPs has prompted us to seek alternative vaccine platforms.

Nearly all plant CPs of icosahedral, positive-sense RNA viruses can be categorized into four distinct structural domains, where the N-terminal "R" domain is involved in the interaction of the viral capsid with genomic RNA [165]. In CMV, the N-terminal fragments of R domains from B and C subunits form a unique bundle of six amphipathic helices oriented down into the virion core case. These helices bind the viral genomic RNA both for its packaging during particle assembly and for maintaining the stability of the assembled particle [166]. This characteristic feature allows the CMV CP N-terminal part (termed here nCMV) to form hexamers post-expression. When fused with a chosen antigen, it may lead to antigen multimerization. Such "immune-tags" [167] may be used as building blocks for vaccine candidates. Furthermore, they provide a novel approach to investigating the individual contributions of Th, PAMPs, and PASPs to the induction of Ab responses.

The use of multimerized N-terminal fragments of CMV CPs containing functional R domains, nCMVs, instead of the entire CuMV$_{TT}$ VLPs offers the versatility of generating multivalent antigens, along with the possibility of attaching TLR-ligands such as RNA. The potential of nCMV as a viable vaccine platform, which we have termed the "Immune-tag" [167], has been investigated here through a mechanistic approach. To this end, the importance of additional Th, PAMPs (TLR7/8 stimulation), and PASPs (antigen multimerization, organization, and repetitiveness) were analyzed both separately and combined. First, the "Immune-tags" carried an enhanced green fluorescent protein (eGFP), serving as a model antigen. eGFP, when used as a "free" antigen, has previously been shown to be poorly immunogenic [168], eliciting only minimal Ab responses, even after the administration of a booster dose [169]. Hence, eGFP may represent a useful protein to demonstrate and quantify the effectiveness of various immunogenicity-enhancing stimuli, including the potential of nCMV-based "Immune-tags".

To further assess the capability of the "Immune-tag"-based vaccine candidate in a context reflecting authentic medical need, we developed a construct targeting dengue virus

1 (DENV-1). This evaluation aimed to determine its ability to elicit DENV-neutralizing Abs, addressing a significant public health concern in warm-climate regions where *Aedes* mosquito vectors are prevalent [170–172]. As an experimental, biologically relevant antigen, we selected the third domain of DENV-1 envelope protein (DV1 EDIII) [173–175], which has been identified to contain several serotype-specific neutralizing epitopes [176–180], indicating that anti-EDIII Abs may have reduced potential to mediate the phenomenon of Ab-dependent enhancement (ADE) [180–183]. In our previous works, we have demonstrated for two other flaviviruses (West Nile and Zika) that the EDIII domain, when expressed alone, folds properly and is capable of inducing neutralizing and protective Abs [60,184].

Our results indicate that antigen multimerization, PAMPs, and extra Th each individually contribute to the elicitation of Ab responses, but the combination of these elements in a non-repetitive antigen carrier does not result in more than an additive increase in response. In contrast, combining all parameters into a highly repetitive, VLP-based vaccine qualitatively enhances the Ab responses. Thus, incorporating PASPs along with extra Th and PAMPs and integrating all stimuli into a single entity was the essential feature for maximal immunogenicity.

2. Materials and Methods

2.1. Cloning of "Immune-Tag" nCMV-eGFP, nCMV-PADRE-eGFP, nCMV-PADRE-DV1 Variants

To create nCMV-containing constructs, a 171 bp long fragment from the wild-type (WT) CMV *CP* gene with an arginine-rich N-terminal domain ([1]MDKSESTSAGRSRRRRPRRGS-RSAPSSADANFRVLSQQLSRLNKTLAAGRPTINHPT[57]), was amplified by PCR using Pfu polymerase (Thermo Fisher Scientific, Waltham, MA, USA) with the oligonucleotides CmN-NcoF and CmN-BamR (Table 1), which contained restriction sites for NcoI (Thermo Fisher Scientific, Waltham, MA, USA) and BamHI (Thermo Fisher Scientific, Waltham, MA, USA), respectively. The pET-CMVwt plasmid [43] was used as the template. The PCR product was extracted from a 0.8% native agarose gel (NAG) using the GeneJet gel extraction kit (Thermo Fisher Scientific, Waltham, MA, USA) following the provided protocol. Subsequently, the PCR fragment was treated with Taq polymerase (Thermo Fisher Scientific, Waltham, MA, USA) to create ddA overlaps for cloning into the ddT of the pTZ57 cloning vector (InsTAclon PCR Cloning Kit, Thermo Fisher Scientific, Waltham, MA, USA). The reaction mixture was prepared according to the protocol, with the addition of 10 mM dATP (Thermo Fisher Scientific, Waltham, MA, USA) instead of the dNTP mix and 10 μL of purified PCR product. The reaction was incubated for 30 min at 72 °C. A linearized pTZ57 ddT vector was then used to clone 1 μL of the reaction mixture, resulting in the creation of the plasmid pTZ-nCMV. The ligates were transformed into XL1-Blue Super competent cells (Agilent Technologies, Santa Clara, CA, USA). Clones containing the insert were verified by Sanger sequencing using the M13seq-F oligonucleotide (Table 1) after test restriction with NcoI and BamHI. The verified pTZ-nCMV clone and a plasmid containing eGFP (pET-eGFP) were cut with HindIII (Thermo Fisher Scientific, Waltham, MA, USA) and BamHI restriction enzymes to clone eGFP at the C-terminus of nCMV, resulting in the development of the pTZ-nCMV-eGFP construct. Subsequently, the nCMV-eGFP and pET-28a(+) (Novagen, Bad Soden, Germany) plasmids were digested with NcoI (partial digestion, as eGFP contains an additional site) and HindIII to develop the pET-nCMV-eGFP expression vector. The constructed vector was selected by digestion with BamHI and HindIII. For rapid purification by Ni^{2+} affinity chromatography, a tag of six histidines (His-tag) was introduced at the C-terminus of eGFP, separated from eGFP by a GGGS flexible linker [185], and the stop codon was removed (note: adding a His-tag at the N-terminal end of nCMV-eGFP reduced expression levels, as indicated by unpublished data). To create this expression vector, two overlapping oligonucleotides, His-tag-C-eGFP-Bsp1407I-F and His-tag-C-eGFP-SacI-R (Table 1), with Bsp1407I and SacI cloning sites (Thermo Fisher Scientific, Waltham, MA, USA), were ordered. Single-stranded oligonucleotide ends were filled by PCR according to the Pfu polymerase protocol, creating a G3S-His-tag PCR

product. The PCR product was purified using the QIAquick PCR Purification Kit (Qiagen, Hilden, Germany) according to the provided protocol. Subsequently, pET-nCMV-eGFP and G3S-His-tag were digested with Bsp1704I and SacI. After fragment purification and ligation, the plasmid pET-nCMV-eGFP was created (Figures 1 and S1A). Correct clones were selected by restriction analysis with BamHI and verified by Sanger sequencing using the pET-rev oligonucleotide (Table 1).

Table 1. Nucleotides used for construct development.

| Oligonucleotide Name	Sequence
CmN-NcoF	5′ ATACCATGGACAAATCTGAATCAACCAGT 3′
CmN-BamR	5′ TCTGGATCCCCGGTTGGGTGGTTAATAGTTGGACGA 3′
His-tag-C-eGFP-Bsp1407I-F	5′ AGCTGTACAAGGGTGGCGGATCCCATCATCATCAT-CATCACCATT 3′
His-tag-C-eGFP-SacI-R	5′ AGCGAGCTCTAGGGCCGCTTTAATGGTGATGATGAT-GATGATGGG 3′
pET-dir	5′ GGGGAATTGTGAGCGGATAACA 3′
pET-rev	5′ TATTGCTCAGCGGTGGCAGC 3′
M13seq-F	5′ GCCAGGGTTTTCCCAGTCACGA 3′
M13seq-R	5′ GAGCGGATAACAATTTCACACAGG 3′
PADRE-eGFP-BamHI-F	5′ ACCACCCAACCGGGGATCCCGCGAAATTTGTGGC-CGCGTGGACCCTC 3′
PADRE-eGFP-AgeI-R	5′ TCACCATGGTGGCCACCGGTGGCGCGGCCGC-CTTGAGGGTCCACGCGGCCAC 3′
nCMV-Vect_R	5′ TGCTCGAGAATTCAAGCTTGCTTTACAATAGCGGTG-GCGCGGCCGCCT 3′
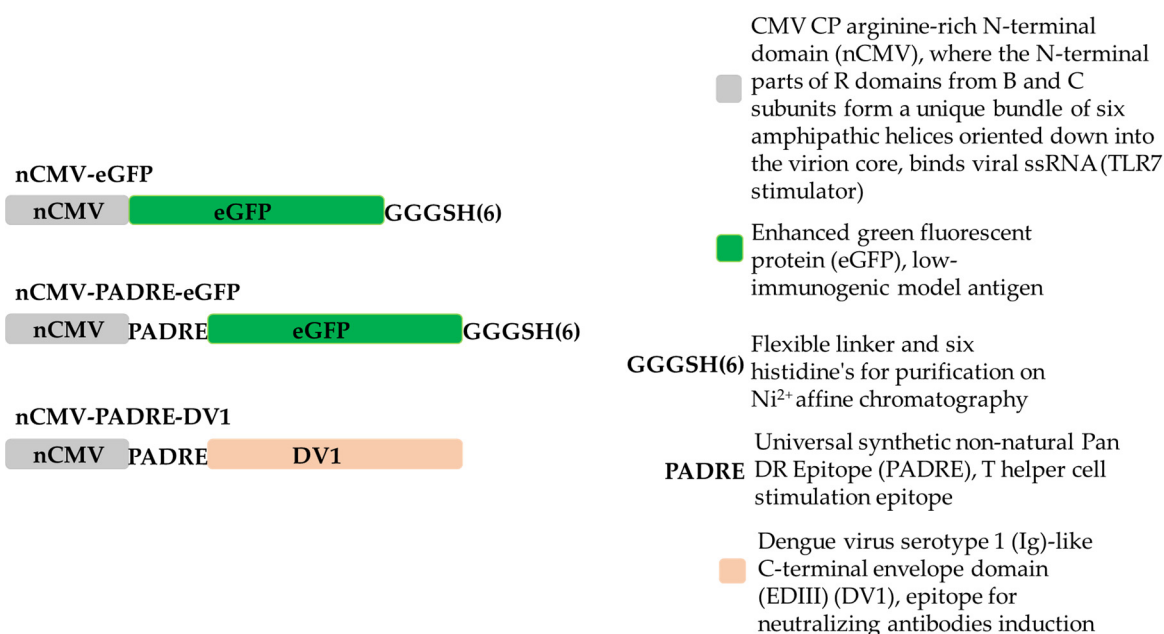
Figure 1. Schematic overview of "Immune-tag" variants used in the study.

To create the PADRE epitope (AKFVAAWTLKAAA [131]) containing construct pET-nCMV-PADRE-eGFP (Figures 1 and S2A), two overlapping oligonucleotides, PADRE-eGFP-BamHI-F and PADRE-eGFP-AgeI-R (Table 1), were used. The same procedure as in the G3S-His-tag case was performed to obtain the PADRE PCR product. Subsequently,

pET-nCMV-eGFP and PADRE were digested with AgeI(BshTI) (Thermo Fisher Scientific, Waltham, MA, USA) and BamHI (partial digestion). Fragments were purified as previously described and ligated. Correct clones were selected by restriction analysis with NotI (Thermo Fisher Scientific, Waltham, MA, USA) and verified by Sanger sequencing using the pET-rev oligonucleotide (Table 1).

To create an "Immune-tag" variant with the DENV-1-derived antigen (DV1 EDIII) at the C-terminus of PADRE, replacing eGFP, we developed a universal cloning vector designed for the insertion of antigens with a NdeI restriction site at their 5′ end. Two overlapping oligonucleotides, PADRE-eGFP-BamHI-F and nCMV-Vect_R (Table 1), were utilized in the procedure identical to that used to obtain the PADRE-Nde PCR product. Subsequently, pET-nCMV and PADRE-Nde were digested with AgeI(BshTI) and XhoI (Thermo Fisher Scientific, Waltham, MA, USA). The DV1 coding sequence was excised from the pET-DV1 construct (ordered by gene synthesis, BioCat, Heidelberg, Germany), using the restriction enzymes NdeI and XhoI, (Thermo Fisher Scientific, Waltham, MA, USA) to obtain the pET-nCMV-PADRE-DV1 construct (Figures 1 and S3A).

2.2. Protein Production, Purification, and Analysis

The created expression vectors pET-nCMV-eGFP, pET-nCMV-PADRE-eGFP, pET-nCMV-PADRE-DV1 were transformed into the C2566 *Escherichia coli* expression strain (New England Biolabs, Ipswich, MA, USA). Cells were cultivated in kanamycin-supplemented 2TY media (Km; 25 μg/mL) and protein expression was carried out according to the developed protocol used in previous studies [43,57,186]. The biomass collected by low-speed centrifugation ($8228\times g$, 5 °C, 5 min) was frozen at −70 °C. Upon thawing on ice, the frozen biomass was suspended in 10 mL of 1× LEW buffer (USB, Cleveland, OH, USA) supplemented with 1 mM phenylmethylsulfonyl fluoride (PMSF; AppliChem, Darmstadt, Germany) and disrupted with ultrasound (Hielscher 200, power 70%, pulse 50%, 16 min) on ice. The solution was clarified by centrifugation ($15,557\times g$, 5 °C, 10 min), and the pellet was discarded. The nCMV-eGFP (Figure S1) and nCMV-PADRE-eGFP (Figure S2) proteins were purified using the PrepEase His-Tagged Protein Purification Midi Kit–High Yield (USB, Cleveland, OH, USA) (Figures S1C and S2C). Elution fractions containing nCMV-eGFP and nCMV-PADRE-eGFP were additionally purified by gel-filtration using an Äkta Pure 25 XK 16/70 column packed with 120 mL Superdex™ 200 (Cytiva, Marlborough, MA USA) (Figures S1D,E and S2D,E). Purified proteins were eluted with PBS at a flow rate of 1 mL/min, collecting 2 mL per fraction. Following analysis by sodium dodecyl sulfate-polyacrylamide gel electrophoresis (SDS-PAGE), 1 mM PMSF was added to the gel-filtrated fractions. The fractions containing nCMV-eGFP and nCMV-PADRE-eGFP were pooled and concentrated using Amicon® Ultra-15, 10 KDa MWCO filtration units (Merck-Millipore, Darmstadt, Germany). The samples were then fresh-frozen and stored at −70 °C.

The cells containing nCMV-PADRE-DV1 (Figure S3) were resuspended in 10 mL of PBS and disrupted as described above. After centrifugation ($15,557\times g$, 5 °C, 10 min), the supernatant was discarded. nCMV-PADRE-DV1 was purified from IB using a single freeze-thawing cycle method [187]. Briefly, pellets containing IB were resuspended in 10 mL of wash buffer (50 mM Tris-HCl pH 8.0, 100 mM NaCl, 1 mM EDTA, 1% TX-100, 1 M urea) by ultrasound (Hielscher 200, power 70%, pulse 50%, 5 min) on ice. IB were collected by centrifugation ($15,557\times g$, 5 °C, 10 min), and the supernatant was discarded. IB washing was repeated two more times. To remove residues of TX-100, IB were washed with PBS. Subsequently, IB were resuspended in solubilization/refolding buffer 100 mM CAPS pH 9.5, arginine 0.9 M, 0.3 mM reduced glutathione (GSH), 0.03 mM oxidized glutathione (GSSG), and 3 M urea and frozen at −20 °C for 16 h. The refolding reaction mixture contains the chaotropic agent, urea, which provides efficient removal of bound impurities from the proteins [188]. Refolded nCMV-PADRE-DV1 was thawed for 1 h at RT on a rotator set at 10 rpm. The supernatant was clarified by centrifugation ($15,557\times g$, 5 °C, 10 min), and the pellet was discarded. nCMV-PADRE-DV1 was dialyzed against 20 mM Na phosphate

buffer, pH 9.0, in a 6–8 kDa dialysis membrane (Spectrum Laboratories, Rancho Dominguez, CA, USA). Additionally, nCMV-PADRE-DV1 was purified by gel-filtration on an Äkta Pure 25 XK 16/70 column packed with 120 mL Superdex™ 200, and purified proteins were eluted with PBS at a flow rate of 1 mL/min, collecting 2 mL per fraction (Figure S3D,E). After analysis by SDS-PAGE, nCMV-PADRE-DV1-containing fractions were pooled and concentrated using Amicon® Ultra-15, 10 KDa MWCO filtration units (Merck-Millipore, Darmstadt, Germany).

eGFP for chemical conjugation was expressed from pQE-eGFP (kindly provided by SIA Asla Ltd.), which was transformed into the *E. coli* C2566 strain. Expression was performed as described above, with minor modifications in the expression step. Cells were grown at 37 °C until an OD600 of 0.8 was reached, then supplemented with 5 mM MgCl$_2$ and induced with 0.2 mM isopropyl-β-D-thiogalactoside (IPTG; Thermo Fisher Scientific, Waltham, MA, USA), and cultivated overnight (ON) at 37 °C and 200 rpm/min (7 × g). The pellet was resuspended in 10 mL of 1× LEW buffer and disrupted with ultrasound (Hielscher 200, power 70%, pulse 50%, 16 min) on ice. The subsequent purification steps were the same as described for nCMV-eGFP and nCMV-PADRE-eGFP (Figure S4).

DV1 EDIII (MW 13.694 kDa) (Figure S5) was purified from IB by a single freeze-thawing cycle method [187] (Figure S5C), as described for nCMV-PADRE-DV1. Instead of the Superdex™ 200 gel-filtration column, Superdex 75™ (Cytiva, Marlborough, MA USA) was used for purification (Figure S5D,E).

All obtained proteins were soluble post-refolding and purification, which supports their structural integrity and native conformation, as proteins lacking correct folding tend to form aggregates [189]. They were subsequently analyzed by 12.5% SDS-PAGE, 0.8% NAG, mass spectrometry (MS), and dynamic light scattering (DLS). Protein concentration was determined using the Qubit 2.0 (Thermo Fisher Scientific, Waltham, MA, USA) with the Qubit™ Protein Assay Kit (Thermo Fisher Scientific, Waltham, MA, USA) following the manufacturer's protocol. All buffers used for the final preparation of protein samples were prepared under sterile conditions, utilizing autoclaved Milli-Q water, and filtered through a 0.22 μm filter.

2.3. Expression and Purification of CuMV and CuMV$_{TT}$ VLPs

The expression and purification of WT CuMV VLPs and "immunologically optimized" CuMV$_{TT}$ VLPs were performed according to the protocols outlined by Zeltins et al. [43], Storni et al. [46], and Sobczak et al. [59]. In summary, RNA was extracted from CMV-infected lily leaves and reverse-transcribed to cDNA. The resultant PCR products were then inserted into the pTZ57R/T vector (Fermentas, Vilnius, Lithuania). Following sequencing, the CMV *CP* gene was transferred into the pET28a(+) vector using NcoI and HindIII restriction sites. For CuMV$_{TT}$, a TT epitope was integrated into the CMV *CP* gene via a two-step PCR-based mutagenesis approach. For protein expression, *E. coli* C2566 cells were transformed with the pET-CuMVwt or pET-CuMV$_{TT}$ plasmid harboring the CuMV or CuMV$_{TT}$ *CP* gene. Collected cell biomass was pelleted by centrifugation (2600× *g*, 4 °C, 10 min), resuspended in lysis buffer, and disrupted using a sonicator (Hielscher UP200S, Amplitude 70%, cycle 0.5) for 16 min. Post-sonication, the lysate was centrifuged (15,000× *g*, 4 °C, 10 min), and self-assembled VLPs were precipitated from the soluble fraction by adding 3 M ammonium sulfate, followed by ON incubation at 4 °C. After subsequent centrifugation (15,000× *g*, 4 °C, 10 min), the pellet was dissolved in sodium borate buffer (5 mM borate, 2 mM EDTA; pH 9.0) and subjected to ultracentrifugation through a 20–60% sucrose gradient (110,000× *g*, 18 °C, 6 h) using a SW32 Ti rotor (Beckman Coulter, Brea, CA, USA). Fractions containing VLPs were further purified twice by ultracentrifugation through a 30% sucrose cushion (250,000× *g*, 4 °C, 4 h) using a Type 70 Ti rotor (Beckman Coulter, Brea, CA, USA) for LPS removal. The pellet obtained after the first ultracentrifugation was dissolved in sodium borate buffer, and the pellet obtained after the second ultracentrifugation was dissolved in VLP storage buffer (5 mM NaP, 2 mM EDTA; pH 7.5) and stored at 4 °C. Quality control was conducted via SDS-PAGE, NAG, and transmission electron

microscopy (TEM). The colorimetric Pierce™ BCA Protein Assay (Thermo Fisher Scientific, Waltham, MA, cat. 23227) was used for the determination of total protein concentration in a final VLP sample. Purified VLPs were tested for endotoxin content, showing less than 100 EU/mg of protein as measured by the Limulus Amebocyte Lysate (LAL) assay (Pierce LAL Chromogenic Endotoxin Quantitation Kit, Thermo Fisher Scientific, Waltham, MA, cat. 88282) [190]. This value is significantly below the endotoxin limits typically set for pharmaceuticals used in mouse models during preclinical research [191,192]. All buffers used for the final preparation of CuMV and CuMV$_{TT}$ VLPs were prepared under sterile conditions, utilizing autoclaved Milli-Q water, and filtered through a 0.22 μm filter.

2.4. Isolation and Quantification of RNA from CuMV Samples

To quantify the RNA content of the VLPs, 250 μL of TRIzol reagent was added to 200 μg of CuMV VLPs and mixed well [193]. The sample was then incubated on ice for 10 min and centrifuged (12,000× *g*, 4 °C, 10 min). The supernatant was transferred to a new tube, and the pellet was discarded. 50 μL of precooled chloroform was added, followed by vortexing for 15 s. The mixture was then incubated on ice for additional 10 min and centrifuged (12,000× *g*, 4 °C, 15 min). The upper aqueous phase was gently transferred to a new tube, avoiding the lower organic phase. Next, 125 μL of ice-cold isopropanol was added to precipitate the RNA. Tubes were inverted 10 times (avoiding vortexing) to mix the contents, followed by a 10 min incubation on ice. The mixture was centrifuged (12,000× *g*, 4 °C, 10 min), and the supernatant was discarded. The RNA pellet was washed with 150 μL of 75% ethanol and gently vortexed. Next, brief centrifugation (8000× *g*, 4 °C, 5 min) was performed to re-pellet the RNA. The supernatant was discarded, and the RNA pellet was dried on a heat block set to 24 °C for 10 min and then resuspended in 100 μL of DEPC-treated water. The pellet was dissolved by gentle pipetting and incubated at 55 °C for 10 min to ensure complete solubilization. The final RNA concentration was determined using a NanoDrop spectrophotometer, showing a yield of 214.5 ng/μL from the initial 200 μg of CuMV, establishing a ratio of roughly 10:1 protein-to-RNA.

2.5. CMV CP mRNA Transcription

To obtain WT CMV *CP* mRNA, 10 μg of the WT CMV *CP*-containing plasmid under the *T7* polymerase promoter created by Zeltins and co-workers [43] was linearized using the HindIII restriction enzyme for 3 h at 37 °C. The linearized plasmid was then purified with a GeneJet gel extraction kit according to the provided protocol, and its concentration was measured using a NanoDrop-1000 spectrophotometer. Subsequently, 1 μg of linearized plasmid was used for WT CMV *CP* mRNA transcription following the TranscriptAid T7 High Yield Transcription kit (Thermo Fisher Scientific, Waltham, MA, USA) manual. Synthesized *CP* mRNA was purified using a GeneJet RNA purification kit (Thermo Fisher Scientific, Waltham, MA, USA) as per the manufacturer's protocol and analyzed on a 1% NAG. The concentration of WT CMV *CP* mRNA was determined using a NanoDrop-1000 spectrophotometer.

2.6. nCMV Binding to Nucleic Acid

To test whether the nCMV is able to bind the nucleic acid, 1 μg of purified WT CMV CP mRNA was incubated with 1 μg of either eGFP, serving as the negative control, or the nCMV-eGFP vaccine [194] for 10 min on ice in their respective storage buffers. Samples were treated with Benzonase® (25 units/μL; Novagen, Bad Soden, Germany) to degrade unbound RNA in the solution. The nucleoprotein complex was analyzed using 0.8% NAG stained with ethidium bromide (Figure S6). Furthermore, the ability of nCMV-PADRE-DV1 to bind the WT CMV *CP* mRNA has been tested with a ratio of 6:1 protein-to-RNA (Figure S3F,G). The 6:1 protein-to-RNA ratio was established to match the equivalent VLP protein-to-RNA ratio, accounting for the potential loss of a small fraction of RNA during isolation from VLPs [195]. This ratio also considers the unknown efficiency of RNA binding

to nCMV "Immune-tags", and is based on the fact that six N-terminal R domains of the CMV CP form a helical bundle upon interacting with RNA.

2.7. Electrophoretic Nucleic Acid Mobility Shift Assay (Gel Shift)

To evaluate the binding capacity of "Immune-tags" to nucleic acids, seven samples of each of the three vaccine variants—eGFP, nCMV-eGFP, and nCMV-PADRE-eGFP—were prepared at seven distinct doses: 0 ng, 150 ng, 300 ng, 600 ng, 800 ng, 1200 ng, and 1500 ng. A uniform concentration of 1 μg per sample of WT CMV *CP* mRNA was introduced to each sample to reach a final reaction volume of 20 μL. Following the addition of the nucleic acid, the samples were chilled on ice for 10 min before being subjected to analysis using a 1% NAG gel. Furthermore, the nCMV-eGFP vaccine variant was tested for its ability to bind to other types of nucleic acids: the CMV CP PCR product, the ryegrass mottle virus (RGMoV) *CP* mRNA, and the Type A CpG TLR9 agonist, G10.

2.8. Development of CuMV-eGFP and CuMV$_{TT}$-DV1 Vaccines

Before chemical conjugation, eGFP lysins were modified with the chemical linker N-succinimidyl S-acetyl thioacetate (SATA; Thermo Fisher Scientific, Waltham, MA, USA) at a 10-molar excess to eGFP following the provided manufacturer protocol. Unreacted SATA and deacetylation solutions were removed using Amicon® Ultra-0.5, 10 KDa MWCO filtration units (Merck Millipore, Darmstadt, Germany). The chemical conjugation of eGFP to WT CuMV VLPs was achieved using the cross-linker succinimidyl 6-((β-maleimidopropionamido)hexanoate)—SMPH (Thermo Fisher Scientific, Waltham, MA, USA; approved for usage in clinical trials [196–198]) at 10-molar excess to WT CMV CP for 1 h at RT. The chemical conjugation reaction was performed by shaking (1400 rpm, RT, 3 h) on a DSG Titertek shaker (Flow Laboratories, Oldham, UK) with a molar ratio of eGFP/CMV CP (1:1). Unreacted SMPH and uncoupled eGFP were removed using Amicon® Ultra-0.5, 100 KDa MWCO filtration units (Merck Millipore, Darmstadt, Germany).

For DV1 chemical conjugation to CuMV$_{TT}$ VLPs, the cross-linker SMPH was used at five molar excesses to CMV CP for 1 h at RT. The chemical conjugation reaction was performed as described above. Unreacted SMPH was removed using Amicon® Ultra-0.5, 100 KDa MWCO (Millipore, Billerica, MA, USA) filtration units. The uncoupled DV1 was removed by gel-filtration on Superdex™ 200 (Cytiva, Marlborough, MA, USA). Concentrations of CuMV-eGFP and CuMV$_{TT}$-DV1 were measured on the ND-1000 and using the Qubit 2.0 (Thermo Fisher Scientific, Waltham, MA, USA). Coupling efficiency was calculated by gel densitometry analysis [43], resulting in approximately 23% for CuMV-eGFP and 17% for CuMV$_{TT}$-DV1 efficiency. Samples were analyzed by SDS-PAGE, NAG, TEM, and DLS.

2.9. Dynamic Light Scattering Measurement (DLS)

VLPs and "Immune-tags" at concentrations of 0.5–1 mg/mL were analyzed in a low-volume glass cuvette (12 μL) using a Zetasizer Nano ZS instrument (Malvern Instruments Ltd., Malvern, UK). The average hydrodynamic diameter of VLPs, or "Immune-tags", was calculated from three consecutive measurements. Results were analyzed by Zetasizer software (version 8.01, Malvern Instruments Ltd., Malvern, UK).

2.10. Sample Analysis by Mass Spectrometry (MS)

Samples for MS analysis were prepared as follows: 2 μL of purified protein (0.5–1 mg/mL) was mixed with 2 μL of 2% trifluoroacetic acid and 2 μL 2,5-dihydroxyacetophenone (2,5-DHAP; Bruker Daltonics, Leipzig, Germany) matrix solution (50 μM 2,5-DHAP dissolved in 96% ethanol and 10 μM aqueous diammonium hydrogen citrate). This mixture was subsequently applied in a volume of 1 μL onto an MTP Anchor Chip 400/384TF (Bruker Daltonics, Leipzig, Germany) and left to crystallize. The sample analysis was performed using an AutoFlex MALDI-TOF MS (Bruker Daltonics, Leipzig, Germany), with mass calibration standard I (Bruker Daltonics, Leipzig, Germany) used for mass calibration.

2.11. Transmission Electron Microscopy (TEM)

5 μL of the sample (1 mg/mL) were adsorbed onto carbon formvar-coated copper grids for 3 min. The grids were then drained by taping one grid edge to the filter paper and washed with 1 mM EDTA. Subsequently, the grids were negatively stained with 5 μL of 0.5% uranyl acetate aqueous solution for 1 min. After staining, the excess staining solution was removed by taping one grid edge to the filter paper and draining in 1 mM EDTA. The grids were examined using a JEM-1230 TEM (JEOL, Tokyo, Japan) at an accelerating voltage of 100 kV or 80 kV.

2.12. Mice

nCMV-eGFP, nCMV-PADRE-eGFP, and CuMV-eGFP immunization experiments were performed using (8–12 weeks old) WT female BALB/c mice purchased from the Laboratory Animal Center at the University of Tartu (Laboratory Animal Center, Tartu, Estonia). All animals were treated for experimentation according to protocols approved by the Animal Protection Ethics Committee of the Latvian Food and Veterinary Service of the Republic of Latvia, permission No. 89, and were conducted in compliance with Directive 2010/63/EU as adopted by the national legislation.

nCMV-PADRE-DV1, CuMV$_{TT}$-DV1, and DV1 EDIII immunization experiments were performed using (8–12 weeks old) WT female BALB/cOlaHsd mice purchased from Envigo (Envigo Rms B.V., Horst, The Netherlands). All experiments were conducted according to protocols approved by the Swiss Cantonal Veterinary Office (license no. BE 70/18).

2.13. Immunization Regimen

The immunogenicity of the created nCMV-eGFP and nCMV-PADRE-eGFP "Immune-tags", as well as their components, in comparison to CuMV-eGFP and "free" eGFP, was tested in mice through subcutaneous (s.c.) injections with a dose of 50 μg diluted in 1× PBS (without adjuvants) up to a total volume of 200 μL. The injection dose was selected based on our previous immunization study with non-adjuvanted VLPs [57] and the reported low immunogenicity of eGFP [168,169]. The mice were divided into six groups (Figure 2), each consisting of five mice: control group (1) received plain eGFP protein, while the experimental groups (2–6) received injections with the following constructs: nCMV-eGFP (2), nCMV-eGFP supplemented with WT CMV *CP* mRNA in a ratio of 6:1 (3), nCMV-PADRE-eGFP (4), nCMV-PADRE-eGFP supplemented with WT CMV *CP* mRNA in a ratio of 6:1 (5), and CuMV-eGFP (6). Booster injections were administered with the same dose for each variant on days 14 and 28. The experiment was terminated on day 42.

The immunogenicity of the created nCMV-PADRE-DV1 "Immune-tag" (supplemented with CMV *CP* mRNA in a 6:1 protein-to-RNA ratio) in comparison to CuMV$_{TT}$-DV1 and "free" DV1 EDIII (Figure 2) was tested in mice by s.c. injections with a dose of either 30 or 10 μg diluted in PBS up to a total volume of 200 μL. These doses were selected based on our previous dose escalation study with a CuMV$_{TT}$-based vaccine [59]. The higher dose (30 μg) aimed to estimate the immunogenicity of developed vaccines, and the lower dose (10 μg) aimed to explore the efficacy of vaccines in inducing a protective immune response measured by an *in vitro* focus reduction neutralization test. Booster injections were performed with the same dose for each variant on day 14. The experiments were terminated on day 35.

The doses of all vaccines were calculated based on the protein content of the active substance. Quantitative analysis of the protein content for each vaccine was performed to ensure accurate dosing and to evaluate the consistency of vaccine formulations. All immunizations were performed with sterile vaccines that were filtered through a 0.22 μm filter.
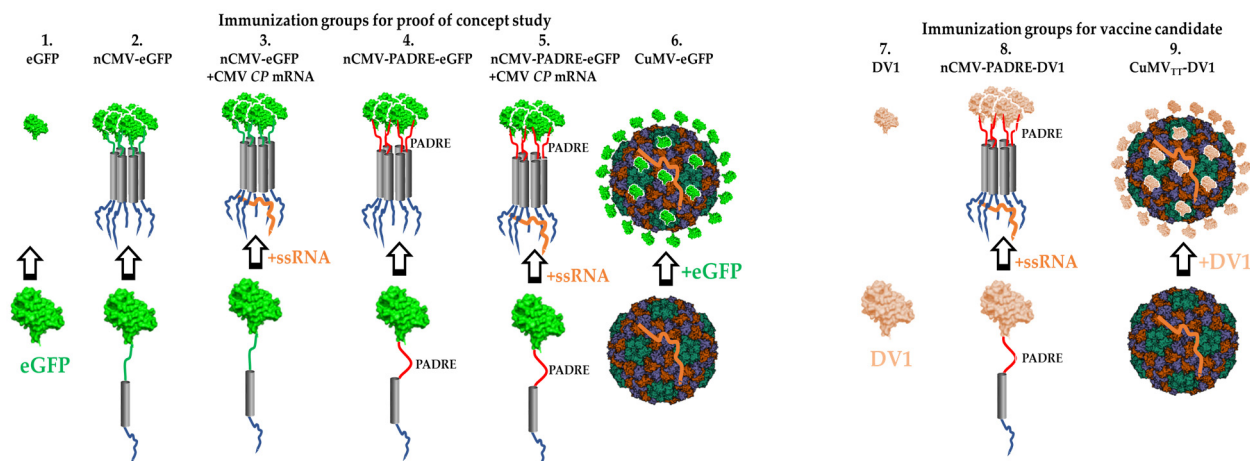
Figure 2. Schematic overview of immunization groups. (**1**) control group immunized with plain eGFP; (**2**) immunized with nCMV-eGFP; (**3**) immunized with nCMV-eGFP supplemented with CMV *CP* mRNA (ssRNA for TLR7 activation) in a protein-to-RNA ratio 6:1; (**4**) immunized with nCMV-PADRE-eGFP; (**5**) immunized with nCMV-PADRE-eGFP supplemented with CMV *CP* mRNA (ssRNA for TLR7 activation) in a protein-to-RNA ratio 6:1; (**6**) immunized with chemically conjugated variant CuMV-eGFP; (**7**) control group immunized with plain DV1; (**8**) immunized with nCMV-PADRE-DV1 supplemented with CMV *CP* mRNA (ssRNA for TLR7 activation) in a protein-to-RNA ratio 6:1; (**9**) immunized with chemically conjugated variant CuMV$_{TT}$-DV1.

2.14. The Enzyme-Linked Immunosorbent Assay (ELISA)

The total IgG Abs titers in the sera of immunized mice against eGFP and WT CMV CP were measured in 96-well ELISA plates (Nunc Immuno MaxiSorp, Rochester, NY, USA, Thermo Fisher Scientific, Waltham, MA, USA) coated either with eGFP or CuMV VLPs diluted in 50 mM sodium carbonate buffer, pH 9.6, at a concentration of 10 μg/mL (100 μL per well), and incubated at 4 °C ON. Plates were washed three times with a washing solution (PBS, 0.05% Tween-20) and then rinsed with dH$_2$O. Subsequently, plates were blocked with 1% BSA in PBS (100 μL per well) at 37 °C for 30 min, followed by washing as previously described. Mouse sera were added to the plates in PBS containing 1% BSA, starting at a dilution of either 1:50 or 1:400. Specifically, a 1:50 pre-dilution was used for sera from mice immunized with either eGFP or "Immune-tag" constructs added to plates coated with either eGFP or CuMV VLPs. A 1:50 pre-dilution was also used for sera from mice immunized with CuMV-eGFP added to plates coated with CuMV VLPs. A 1:400 pre-dilution was used for sera from mice immunized with CuMV-eGFP added to plates coated with eGFP. Serial dilutions of pre-diluted sera were performed with a dilution ratio of 1:2. Plates were incubated at 37 °C for 1 h, followed by washing as before. Rabbit anti-mouse IgG, conjugated with horseradish peroxidase (HRP) (Sigma–Aldrich, St. Louis, MO, USA, cat. A9044-2ML), was added at a dilution of 1:10,000 (100 μL per well). Plates were incubated at 37 °C for 1 h and washed as previously described. The OPD substrate tablet (o-phenylenediamine dihydrochloride; Sigma–Aldrich, St. Louis, MO, USA) was dissolved in 10 mL of 50 mM sodium carbonate buffer, pH 9.6, with the addition of 15 μL of H$_2$O$_2$. Then, 100 μL of substrate solution was added to each well, and plates were incubated at 37 °C for 20 min. The reaction was terminated by adding 1.2 N H$_2$SO$_4$ in a volume of 50 μL per well. Optical absorbance was measured at 492 nm (OD492) using a Labsystems Multiskan MS Type 352 microplate reader (Labsystems Diagnostics Oy, Vantaa, Finland). The endpoint titers were calculated as the highest serum dilution that resulted in an absorbance value exceeding three times that of the negative control (serum obtained from non-immunized mice) [199,200].

Isotype-specific ELISA was performed using the mouse monoclonal Ab isotyping reagent ISO2 (Sigma–Aldrich, St. Louis, MO, USA, cat. ISO2-1KT) and a secondary anti-goat/sheep IgG, HRP Abs (Sigma–Aldrich, St. Louis, MO, USA, cat. A9452-1VL). For

the determination of IgG1 and IgG2a subclass levels in the sera of mice immunized with constructs containing eGFP, the following Abs were used in ELISA: goat anti-mouse IgG1, HRP (1:1000) (Thermo Fisher Scientific, Waltham, MA, USA, cat. PA1-74421) and goat anti-mouse IgG2a, HRP (1:1000) (Thermo Fisher Scientific, Waltham, MA, USA, cat. A-10685). Endpoint titers were calculated as described previously.

Total IgG Abs titers in sera of immunized mice against DV1 EDIII were measured in 96-well half-area ELISA plates (Corning Inc., Corning, NY, USA) coated with DV1 EDIII diluted in $1\times$ PBS with a concentration of 2 μg/mL (50 μL per well), incubated at 4 °C ON. On the following day, plates were washed five times with PBS and blocked with 0.15% casein in PBS (100 μL per well) at RT for 2 h followed by washing as previously described. Mouse sera were added to the plates in PBS containing 0.15% Casein, starting at a dilution of either 1:30 or 1:10. Specifically, a 1:30 pre-dilution was used for sera from mice immunized with 30 μg of either DV1 EDIII, nCMV-PADRE-DV1, or CuMV$_{TT}$-DV1. A 1:10 pre-dilution was used for sera from mice immunized with 10 μg of either nCMV-PADRE-DV1 or CuMV$_{TT}$-DV1. Serial dilutions of the pre-diluted sera were then performed with a dilution ratio of either 1:5 or 1:3, respectively. Plates were incubated at RT for 1.5 h and washed as previously. Subsequently, a goat anti-mouse IgG conjugated to HRP (Jackson ImmunoResearch, West Grove, PA, USA; cat. 115 035 008) was added with a dilution factor of 1:5000 and incubated at RT for 1 h. Following incubation, plates were washed five times with PBS-Tween 0.01%. The ELISA was developed with a 50 μL solution of tetramethylbenzidine (TMB), H_2O_2, and acetate buffer (pH 4.1). The reaction was terminated after 5 min by the addition of 50 μL of 1 M H_2SO_4 per well. Optical absorbance was measured at an OD of 450 nm (OD450) on an ELISA plate reader. Half-maximal Ab titers (OD$_{50}$) were defined as the reciprocal of the dilution leading to half of the OD measured at saturation.

The avidity of vaccine-induced DV1 EDIII-specific IgG was tested through the avidity ELISA assay performed by extending the ELISA protocol with additional washing steps with a chaotropic agent—urea [55,56,164,201]. Following serum incubation with a pre-dilution of 1:20 and serial dilution of 1:3, the plates were washed with PBS containing 0.01% Tween. The plates were then incubated three times with 7 M urea in PBS containing 0.01% Tween for 5 min on a shaker at RT, or with PBS containing 0.01% Tween as a control. Between these incubations, plates were washed again with PBS-Tween 0.01%. The avidity index (AI) was calculated by the ratio of dilution factors (titers) with and without urea denaturation [202–204].

2.15. DENV-1 Focus Reduction Virus Neutralization Test (FRNT)

The DENV-1 neutralization capacity of antibodies produced after immunizing mice was determined using focus reduction virus neutralization test (FRNT). Human convalescent serum 001 to Dengue Virus (NR-50226) was used as positive control, while sera from naïve mice were used as a negative control. Briefly, a day before the experiment 96-well substrate plate was prepared using Vero cells (2×10^4 cells/well) cultured in complete media. The sera from vaccinated mice were heat-inactivated (HI) at 56 °C for 30 min to inactivate complement and diluted 1:100 in infection media (composition: DMEM supplemented with 0.75% NaHCO$_3$, 10 mM HEPES buffer, 1% Pen-Strep, and 1% HI-FBS). The 500 TCID50 of DENV-1 (VR1856, Hawaii) was added to each well in an equal volume and the mixture was incubated at 37 °C for 1 h. The mixtures of virus and sera were then added to the substrate plate and incubated for 1 h at 37 °C in 5% CO$_2$. Subsequently, the cell monolayers were washed once with PBS followed by the addition of the infection media and incubated at 37 °C in 5% CO$_2$ for another 48 h. To determine the number of virus-infected cells an in-house developed immunostaining method was used. Briefly, the infected cells were fixed with 2.5% formalin and permeabilized with 0.1% Triton X-100 in 70% ethanol. The infected cells were stained with Rabbit anti-flavivirus group antigen monoclonal antibody (Absolute antibody, Oxford, UK) and detected with Goat anti-rabbit IgG (H+L) Highly Cross-Adsorbed Secondary Antibody, Alexa Fluor Plus 488 (2 mg), (Invitrogen, Waltham, MA, USA). Following this, wells were incubated with 4′,6-Diamidino-2-Phenylindole, Di-

hydrochloride (DAPI) (Thermo Fisher Scientific, Waltham, MA, USA) to counterstain the nucleus. Plates were scanned using Cytation 1 Imaging Reader (BioTek, Winooski, VT, USA) at a 4× objective and analysed by the Gen5 software (BioTek, Winooski, VT, USA). The percentage reduction of DENV-1-infected cells was determined by comparing the number of infected cells to the negative control. Each serum sample was tested in duplicate.

2.16. Data Analysis

Statistical analysis of the collected data was conducted using GraphPad Prism Version 8 (Graph Pad Software Inc., San Diego, CA, USA). For comparisons among groups exhibiting a normal distribution, Student's *t*-tests or ANOVA were used, incorporating Welch's correction for the assumptions of unequal variances across groups. For groups not following a normal distribution, the Kruskal-Wallis nonparametric test was used. Differences between groups with *p*-values of 0.05 or less were considered statistically significant (* $p \leq 0.05$, ** $p \leq 0.01$, *** $p \leq 0.001$, and **** $p \leq 0.0001$).

3. Results

3.1. Development of "IMMUNE-TAG" as a Vaccine Platform

To dissect the roles of PAMPs, PASPs, and Th stimulation in driving B cell responses, we designed the nCMV as a novel vaccine platform, the "Immune-tag" [167]. Our investigation focused on its ability to oligomerize post-purification and to elicit Ab responses against model antigens, enhanced by the addition of TLR and T-cell-stimulating epitopes. The "Immune-tag" design facilitates swift antigen replacement, cost-effective purification, and the incorporation of immunostimulating components. To begin with, we developed two "Immune-tag" constructs to examine their feasibility. In the first construct, the C-terminal part of nCMV was genetically fused to eGFP (nCMV-eGFP; Figures 1, 2 and S1), while the second incorporated an additional PADRE epitope between nCMV and eGFP (nCMV-PADRE-eGFP; Figures 1, 2 and S2). Both "Immune-tag" variants were expressed in *E. coli* at high concentrations and in soluble form (Figures S1C and S2C). "Immune-tags" and a "free" eGFP serving as a control were analyzed on SDS-PAGE (Figure 3A) and by MS (Figure 3B) after purification and concentration. During MS analysis, partial proteolysis of nCMV-PADRE-eGFP was observed, revealing two peaks: one corresponding to the full length of nCMV-PADRE-eGFP (36.47 kDa) and the second to the eGFP (29.36 kDa) (Figure 3B). The addition of protease inhibitors such as PMSF was sufficient to protect the construct against proteolysis after the gel-filtration step (Figures 3A and S2D), which allowed for the separation of the intact nCMV-PADRE-eGFP from a processed part. On the other hand, the MS analysis demonstrated the integrity of the nCMV-eGFP "Immune-tag" with a corresponding size of 35.03 kDa (Figure 3B).

To assess the capacity of nCMV for nucleic acid binding, gel shift assays were conducted. The assays revealed a migration delay in WT CMV *CP* mRNA in NAG, indicating the retained ability of nCMV to bind mRNA encoding WT CMV CP (Figures S1F and S2F). Considering that the binding of nucleic acids by nCMV relies on electrostatic interactions, these results suggested that nCMV had the potential to bind nucleic acids from various sources. To examine this feature of nCMV, we tested the effect of supplementing nCMV-eGFP with WT CMV *CP* PCR product, as well as RGMoV *CP* mRNA [205], and with Type A CpG TLR9 agonist—G10 [206,207], observing the same migration delay of the construct as for WT CMV *CP* mRNA (Figure S7). Further analysis of the nCMV-eGFP and nCMV-PADRE-eGFP constructs, both with and without RNA, was performed using DLS and TEM. These techniques verified the oligomer formation (Figures S1G–J and S2G–J), with the prospective ability to facilitate augmented Ab responses against target antigens. Both "Immune-tag" variants, enriched with WT CMV *CP* mRNA, were used in subsequent mouse immunization experiments to examine whether nCMV oligomerization and supplementation with TLR7/8 ligand could serve as self-adjuvants.
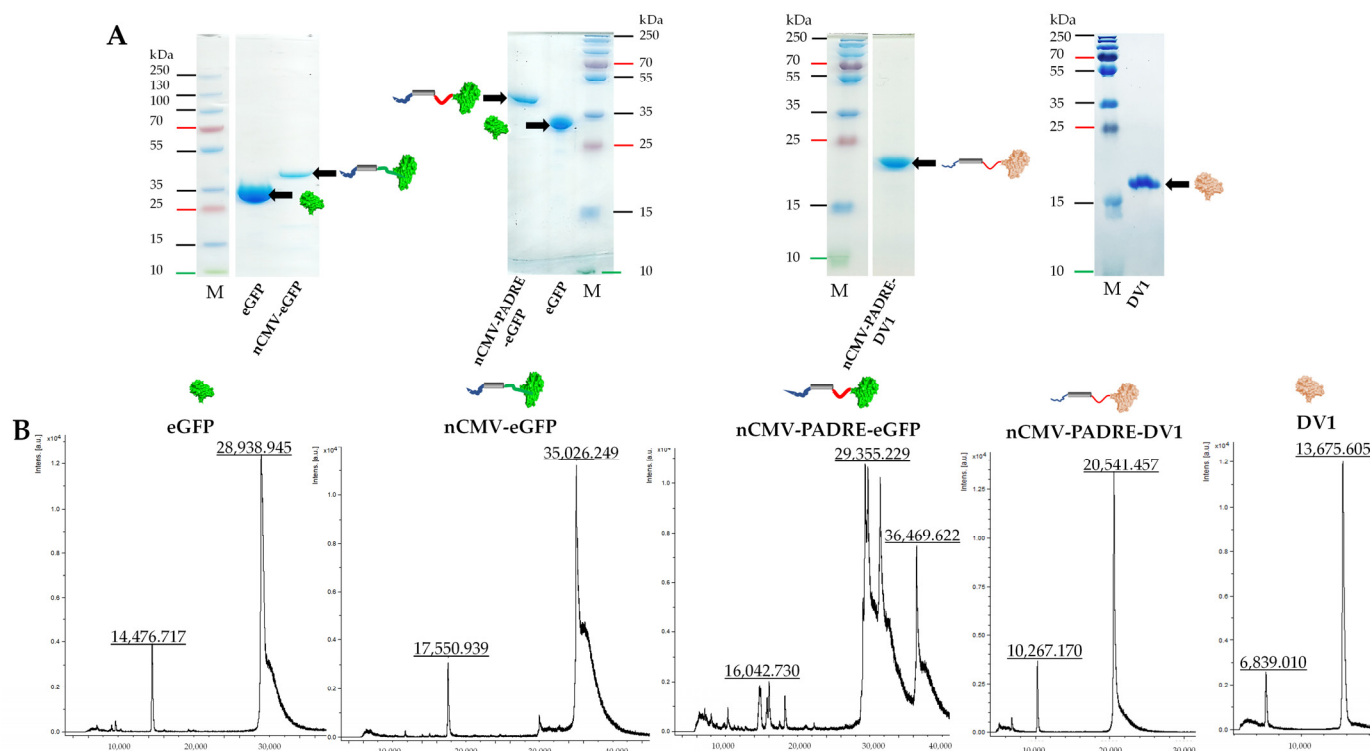
Figure 3. Molecular mass and integrity analysis of developed "Immune-tags". (**A**)—SDS-PAGE stained with Coomassie G250 stain; M—protein molecular weight marker (PageRuler^{TM} Plus, Thermo Fisher Scientific, Waltham, MA, USA, cat. 26619); eGFP—enhanced green fluorescent protein (MW 29 kDa); nCMV-eGFP (MW 35 kDa); nCMV-PADRE-eGFP (MW 36.5 kDa); nCMV-PADRE-DV1 (MW 20.5 kDa); DV1—immunoglobulin (Ig)-like C-terminal domain of the DENV-1 envelope protein (EDIII) (MW 13.7 kDa); (**B**)—mass spectrometric analysis of the purified "free" proteins and "Immune-tag" constructs.

To employ another antigen, in exchange to the model eGFP antigen (Sections 3.3–3.5), the "Immune-tag" was adapted for DENV-1. In this adaptation, the DV1 EDIII sequence derived from DENV-1 (Figure S5A) was integrated into the platform by replacing eGFP, thus creating a new construct, nCMV-PADRE-DV1 (Figure S3B). Both the nCMV-PADRE-DV1 "Immune-tag" (Figure S3) and "free" DV1 EDIII (Figure S5) following purification were analyzed on SDS-PAGE and by MS (Figure 3), to confirm the integrity and expected molecular properties of the nCMV-PADRE-DV1 construct. Before immunization, nCMV-PADRE-DV1 was supplemented with CMV *CP* mRNA in a protein-to-RNA ratio of 6:1 (Figure S3F,G).

3.2. Chemically Modified VLP-Based Platform

The comparative analysis aimed to understand the impact of antigen spatial organization and repetitiveness (PASP) on the efficiency of Ab induction and was conducted utilizing a selected model antigen—eGFP. eGFP was either genetically fused with the "Immune-tags" or chemically coupled to the surface of structurally uniform VLPs (Figure 2). To compare their immunological potentials without additional confounding variables, eGFP was conjugated to VLPs derived from WT CMV (CuMV), lacking integration with TT epitopes. This design avoids direct comparison between the PADRE and the TT CD4+ epitopes, thereby allowing a clearer assessment of the influence of antigen organization and repetitiveness against other B-cell stimulatory features incorporated into the "Immune-tag" constructs.

In the second phase of the project, when focusing principally on identifying a potent vaccine candidate against DENV-1, DV1 EDIII antigen was conjugated with "immunologically optimized" VLPs (CuMV$_{TT}$), which do incorporate a universal T-cell epitope from

TT. This fusion aims to boost the interaction between Th cells and B cells and has been shown to significantly enhance Ab responses in mice that were primed with TT before being immunized with CuMV$_{TT}$ [59,160]. In essence, the incorporation of the TT epitope is designed to leverage the widespread pre-existing immunity to TT within the human population, potentially leading to improved vaccine effectiveness, especially in specific groups such as elderly patients.

The expression levels, purity, and efficiency of the conjugation process of eGFP to WT CuMV CP and DV1 to CuMV$_{TT}$ CP were evaluated using 4–12% SDS-PAGE and 0.8% NAGE. The latter revealed successful conjugation of eGFP and DV1 to VLPs, as evidenced by the altered mobility of VLPs in the gel (Figure 4). Further confirmation of antigen-VLP conjugation quality was obtained through SDS-PAGE analysis, where a characteristic ladder could be observed, indicating a successful conjugation reaction (Figure 4). To assess the structural integrity and uniformity of the antigen-conjugated VLPs, TEM and DLS analyses were employed. TEM images demonstrated that the VLPs remained intact following the conjugation procedure. DLS analysis showed the presence of homogeneous peaks with average hydrodynamic diameters (D$_h$) of about ~61 nm for CuMV-eGFP and ~46 nm for CuMV$_{TT}$-DV1 (Figure 4).
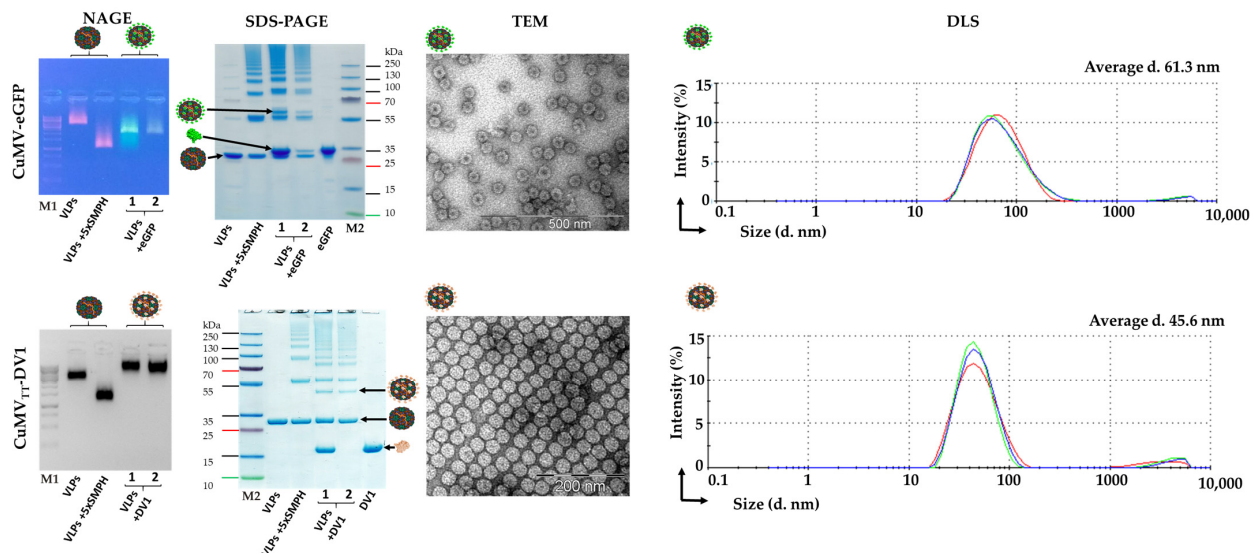

Figure 4. Integrity analysis of antigen coupling to VLPs. NAGE—coupling analysis in 0.8% native agarose gel electrophoresis, gel stained with ethidium bromide; bands indicate the presence of prokaryotic nucleic acid (mRNA) encapsulated inside the VLPs; SDS-PAGE—coupling analysis by 4–12% BoltPAGE stained with Coomassie G250, as a result of subunit crosslinking, derivatization by SMPH leads to the characteristic ladder of VLP monomers, dimers, trimers, tetramers, etc., indicating successful coupling reaction; TEM—analysis of VLPs after coupling by transmission electron microscopy at 80× (upper panel) or 100× (lower panel) magnifications; DLS—analysis of the uniformity and hydrodynamic diameter of VLPs after coupling by dynamic light scattering. Lanes in NAGE and SDS-PAGE: VLPs—uncoupled particles (negative control); VLPs + 5×SMPH— VLPs bound to the crosslinker (negative control); VLPs + eGFP/DV1: 1—VLPs loaded directly after coupling with antigen; 2—coupled VLPs loaded after removal of "free" (uncoupled) antigen; eGFP/DV1—"free" protein/peptide; M1—1 kb DNA ladder (GeneRuler^{TM} 1 kb, Thermo Fisher Scientific, Waltham, MA, USA, cat. SM0311); M2—protein molecular weight marker (PageRuler^{TM} Plus, Thermo Fisher Scientific, Waltham, MA, USA, cat. 26619).

3.3. Characterization of the Immunogenic Potential of nCMV–eGFP Using "Immune-Tag" Technology

The efficacy of the immune response to a vaccine is significantly influenced by virus-like features. PAMPs and structural patterns such as size, geometry, and the presence of highly repetitive and ordered surface patterns (PASPs) play a crucial role in mimicking the natural attributes of viruses [3]. Some studies argue that simplified versions of VLPs, e.g., self-assembled viral nanostructures, may also serve as viral mimetics [208,209]. It can be hypothesized that incorporating additional immunostimulatory components into the "Immune-tag" nCMV-eGFP could increase Ab titers induced against the eGFP. This approach would facilitate the identification of the optimal configuration for future vaccine candidates utilizing the "Immune-tag"-based platforms.

The immunogenicity of the developed eGFP-carrying nCMV "Immune-tag" constructs (Figures 1 and 2) was evaluated through a vaccination regimen consisting of s.c. priming followed by two booster doses administered at 14-day intervals. To assess the impact of immunostimulatory elements on the immune response, we incorporated the PADRE element with the "Immune-tag" and/or supplemented it with ssRNA. For comparison, a "free" eGFP as well as CuMV-eGFP VLPs were used in the study (Figure 2). Serum samples from the mice were collected before the administration of the first dose and again at the endpoint of the study on Day 42. The total serum IgG levels as well as IgG1 and IgG2a subclasses against both eGFP and CuMV VLPs were measured by ELISA with the collected sera.

3.4. Total Levels of Anti-eGFP IgG

There was a clear hierarchy in the eGFP-specific IgG responses. Groups of mice immunized with eGFP alone produced the lowest anti-eGFP IgG antibody titers, with mean reciprocal titers of 1:193 (Figure 5A,B). This result is consistent with the concept that oligomerization or multimerization of proteins into complexes can enhance immunogenicity by improving antigen recognition [210].

In comparison to eGFP alone, the experimental groups immunized with nCMV-based vaccines against eGFP exhibited a 4- to 14-fold increase in anti-eGFP IgG Ab titers (Figure 5A,B). The addition of each immunostimulatory element contributed to this rise in Ab titers. Interestingly, PADRE and RNA, when added individually, similarly boosted Ab responses, while the addition of both elements concurrently did not exhibit synergistic or even additive combined effects and resulted in a similar increase as the addition of each individual element separately. Importantly, the total eGFP-specific IgG titers in the group immunized with CuMV-eGFP VLPs were an order of magnitude higher than those measured in any other group, reaching mean reciprocal titers of 1:56,536 (Figure 5A,B). This suggests that the most effective immune responses are elicited when all viral components and features are integrated into a single entity.

CMV CP-specific IgG were detected exclusively in the sera of mice immunized with CuMV-eGFP (Figure S8). This observation is likely due to the nCMV fragment of CMV CP being concealed inside the particle.
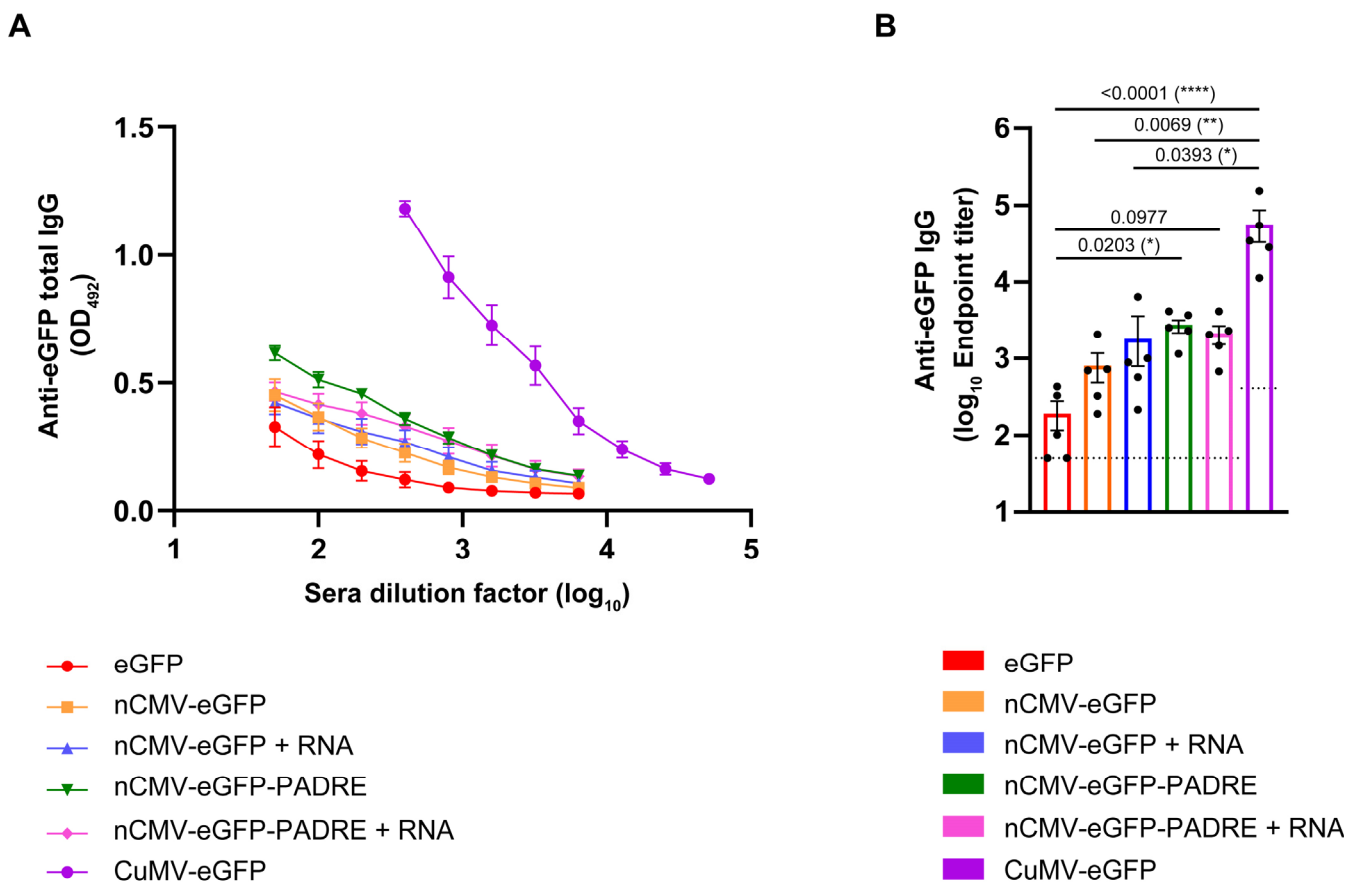
Figure 5. Analysis of eGFP-specific IgG titers following vaccination with vaccine variants. (**A**)—eGFP-specific IgG titers on day 42 for the groups vaccinated with nCMV-eGFP variants and CuMV-eGFP, measured at OD 492 nm; (**B**)—$\log_{10}$ of eGFP-specific IgG endpoint titers for the groups vaccinated with nCMV-eGFP variants and CuMV-eGFP. Statistical analysis (mean ± SEM) using the Kruskal-Wallis test. Vaccinated groups: *n* = 5. One representative experiment is shown. A value of $p \leq 0.05$ was considered statistically significant (* $p \leq 0.05$, ** $p \leq 0.01$, *** $p \leq 0.001$, **** $p \leq 0.0001$).

3.5. Subclass-Specific Anti-eGFP IgG Antibodies

Literature underlines the importance of isotype class switching, IgG subclass differentiation, and the presence of high-affinity Abs as key factors influencing vaccine efficacy [211,212]. Specifically, IgG1 and IgG2a Ab subclasses serve as indicators of Th2 or Th1 responses, respectively. IgG2a rather than IgG1 engages activating Fc receptors, typically correlating with enhanced vaccine effectiveness [213,214]. The subclass-specific Ab response may strongly depend on TLR-stimulating factors such as RNA or DNA [215]. The preferential induction of IgG1 Abs was observed for influenza M2e domain-derived tetramers used for immunizations in BALB/c mice [216]. Conversely, Wang and co-workers [217] claimed that oligomers expressed by a DNA-based vaccine derived from the *Yersinia pestis* V antigen, which included a signal sequence from a human tissue plasminogen activator, elicited a dominant IgG2a response in the BALB/c murine model [217]. A similar observation was reported by Dalgediene and co-workers [218], where immunization of mice of the same strain with a polypeptide, the beta-amyloid (Aβ) oligomer, induced a predominantly IgG2a response [218]. These results indicate the importance of the origin of the oligomeric structures (e.g., viral, bacterial, fungal, mammalian, or self-created) in the stimulation of diverse IgG subclass responses, presumably via stimulation of different TLRs. To assess whether the developed "Immune-tags" could induce either IgG1 or IgG2a subclass-specific antibodies, blood sera from day 42 were analyzed.

Analysis of the Ab responses revealed a predominance of anti-eGFP IgG1 Abs across all tested groups. The highest response was observed in the group of mice immunized with chemically coupled CuMV-eGFP VLPs, achieving mean reciprocal titers of 1:15,131 (Figure 6A,B). When comparing nCMV-based "Immune-tags" to eGFP alone, a similar pattern of a 2- to 9-fold increase in eGFP-specific IgG1 Ab titers was observed, consistent with the measurements of total anti-eGFP IgG. This indicates that the majority of the detected total IgG was indeed of the IgG1 subclass. These findings align with a previously reported study, which identified IgG1 as the most prevalent Ab subclass in response to soluble protein antigens in mice [219–222].
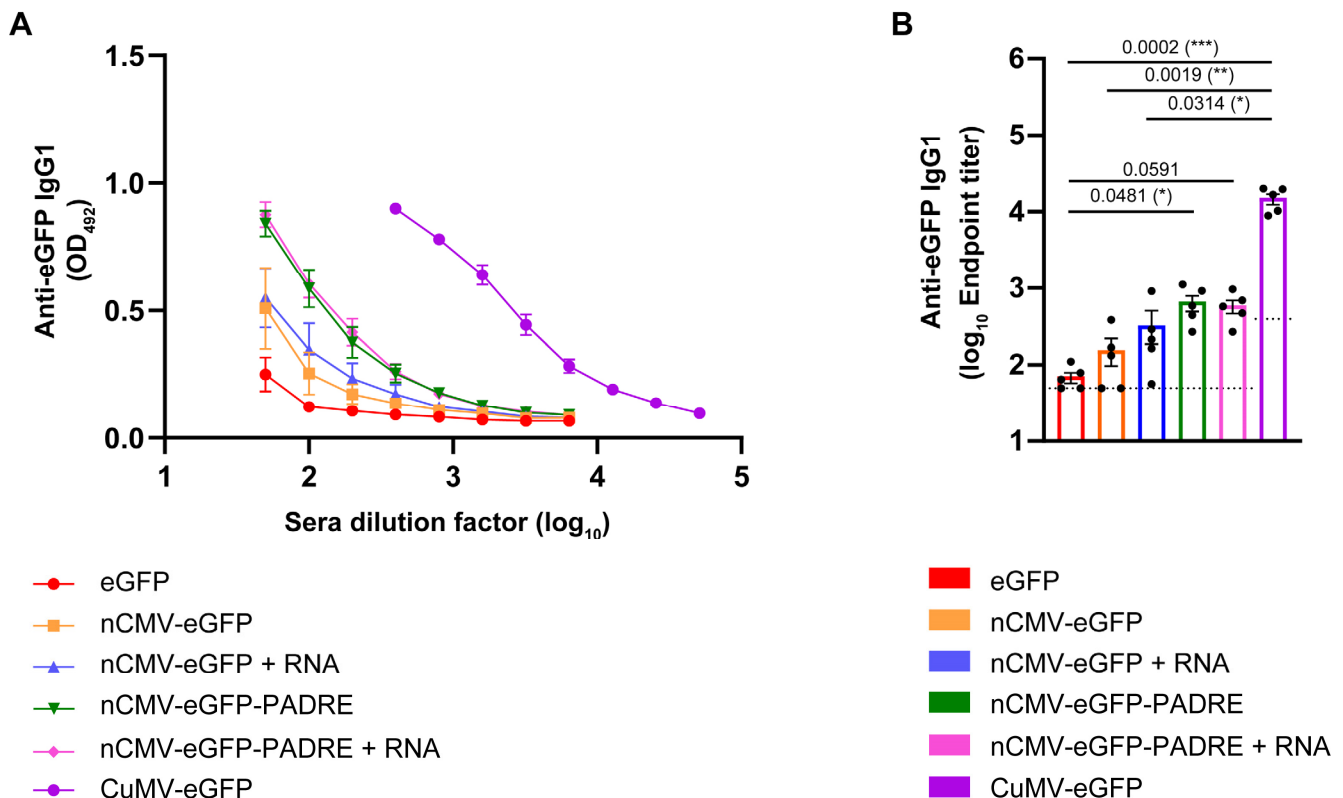

Figure 6. Induction of subclass switching to IgG1 by nCMV-eGFP variants and CuMV-eGFP determined by ELISA analysis. (**A**)—anti-eGFP-specific IgG1 titers measured on day 42 in mouse sera at OD 492 nm. (**B**)—$\log_{10}$ values of eGFP-specific IgG1 titers for the groups vaccinated with nCMV-eGFP variants and CuMV-eGFP. Statistical analysis (mean ± SEM) using the Kruskal-Wallis test. Vaccinated groups: *n* = 5. One representative experiment is shown. A value of $p \leq 0.05$ was considered statistically significant (* $p \leq 0.05$, ** $p \leq 0.01$, *** $p \leq 0.001$, **** $p \leq 0.0001$).

eGFP-specific IgG2a Abs were detected only in the sera of mice vaccinated with CuMV-eGFP, reaching mean reciprocal titers of 1:2020 (Figure S9). These results suggest that constructed "Immune-tags" lack components that stimulate IgG2a production, in contrast to vaccines derived from whole VLPs. This aligns with previous findings that viruses induce IgG2a response in mice [221,222] and suggests that CP structural elements, when presented as multimerized "Immune-tags", may not be recognized by the immune system in the same manner as the whole particle containing encapsulated nucleic acid.

3.6. nCMV-PADRE "Immune-Tag" as a Dengue Vaccine Candidate

To answer the question of whether the nCMV-PADRE "Immune-tag" may serve as an alternative platform for vaccine development, the immunogenicity of this construct was verified as a model anti-viral vaccine. For this purpose, the nCMV-PADRE was genetically fused with the DV1 EDIII (nCMV-PADRE-DV1; Figures 1 and 2; Section 3.1). The Ig-like

C-terminal EDIII of the DENV is known to be involved in the association of a virion with a receptor expressed on the surface of a host cell [223], serving as a crucial structure in viral entry. Consequently, EDIII contains epitopes that are exposed on the surface of the virion, constituting natural targets for the generation of neutralizing Abs [223,224].

The immunogenicity of the newly constructed "Immune-tag" nCMV-PADRE-DV1 was evaluated in BALB/c mice. Animals were immunized s.c. with a 30 µg dose on Day 0, followed by a booster administered on Day 14. As negative and positive controls, the soluble DV1 EDIII and DV1 EDIII chemically coupled to the previously described "immunologically optimized" $CuMV_{TT}$ ($CuMV_{TT}$-DV1) [43] were used, respectively. The titers of serum total anti-DV1 EDIII IgG were measured at the endpoint of the experiment on Day 35 to assess the consistency of the IgG response hierarchy. Indeed, the IgG levels induced by the nCMV-PADRE-DV1 were higher than those in mice immunized with DV1 EDIII alone, confirming the relatively lower immunogenicity of the protein vaccines based on the recombinant DENV EDIII. Consistent with findings from the use of the eGFP model antigen, the anti-DV1 EDIII IgG levels were significantly highest in the group immunized with $CuMV_{TT}$-DV1 (Figure 7A,B).

To compare the collective binding potency of the polyclonal serum anti-DV1 EDIII IgG Abs induced by $CuMV_{TT}$-DV1, nCMV-PADRE-DV1, and DV1 EDIII alone, we performed an avidity ELISA assay. This assay was designed to include three intermediate 5-min plate washes with 7 M urea to reveal the differences between groups based on their specific IgG avidity. The use of this chaotropic agent eliminated low-affinity Abs from the samples (Figure 7C,D). The calculated AI revealed that nCMV-PADRE-DV1 induced significantly higher levels of high-affinity DV1 EDIII-specific IgG compared to "free" DV1 EDIII protein, while $CuMV_{TT}$-DV1 induced the highest ratio of such IgGs of all vaccine candidates used (Figure 7E).

Subsequently, BALB/c mice were immunized s.c. with a 10 µg dose of the "Immune-tag" nCMV-PADRE-DV1 or $CuMV_{TT}$-DV1 following the same prime/boost regimen as shown before in Figure 7. Serum samples were collected before the prime on day 0, before the booster on day 14, as well as after the booster on days 21 and 35. A significantly higher levels of serum anti-DV1 EDIII IgG were observed on both day 14 and day 35 in the group of mice immunized with $CuMV_{TT}$-DV1. Interestingly, after the boost, on day 21, the difference in levels of serum anti-DV1 EDIII IgG between the two groups was not significant (Figure 8A,B). This observation indicates that while $CuMV_{TT}$-DV1 induced a stronger initial and longer-term IgG response against DV1 EDIII, during the immediate post-boost period there was no substantial difference in Ab levels between those two vaccine candidates.

Serum samples from mice immunized with 10 µg of oligomeric nCMV-PADRE-DV1 and $CuMV_{TT}$-DV1 VLPs collected on Days 14, 21, and 35 were analyzed using a DENV-1 FRNT to assess the neutralizing capability of the Abs elicited by both vaccine constructs. The effectiveness of these Abs in neutralizing DENV-1 was determined by measuring the reduction in the number of virus-infected Vero cells in vitro, compared to a baseline established using cells infected by the virus incubated with pre-immune serum (collected on day 0). The results demonstrated that both vaccines were capable of inducing Abs that neutralized DENV-1 following the booster dose administered on day 21, as shown in Figure 9. However, the response induced by the oligomeric nCMV-PADRE-DV1 was found to be very transient, whereas the response from the VLP-based $CuMV_{TT}$-DV1 vaccine was significantly more sustained. By day 35, the neutralizing capability of Abs induced by $CuMV_{TT}$-DV1 was significantly greater than that induced by nCMV-PADRE-DV1, indicating a more durable protective effect with the VLP-based vaccine (Figure 9).
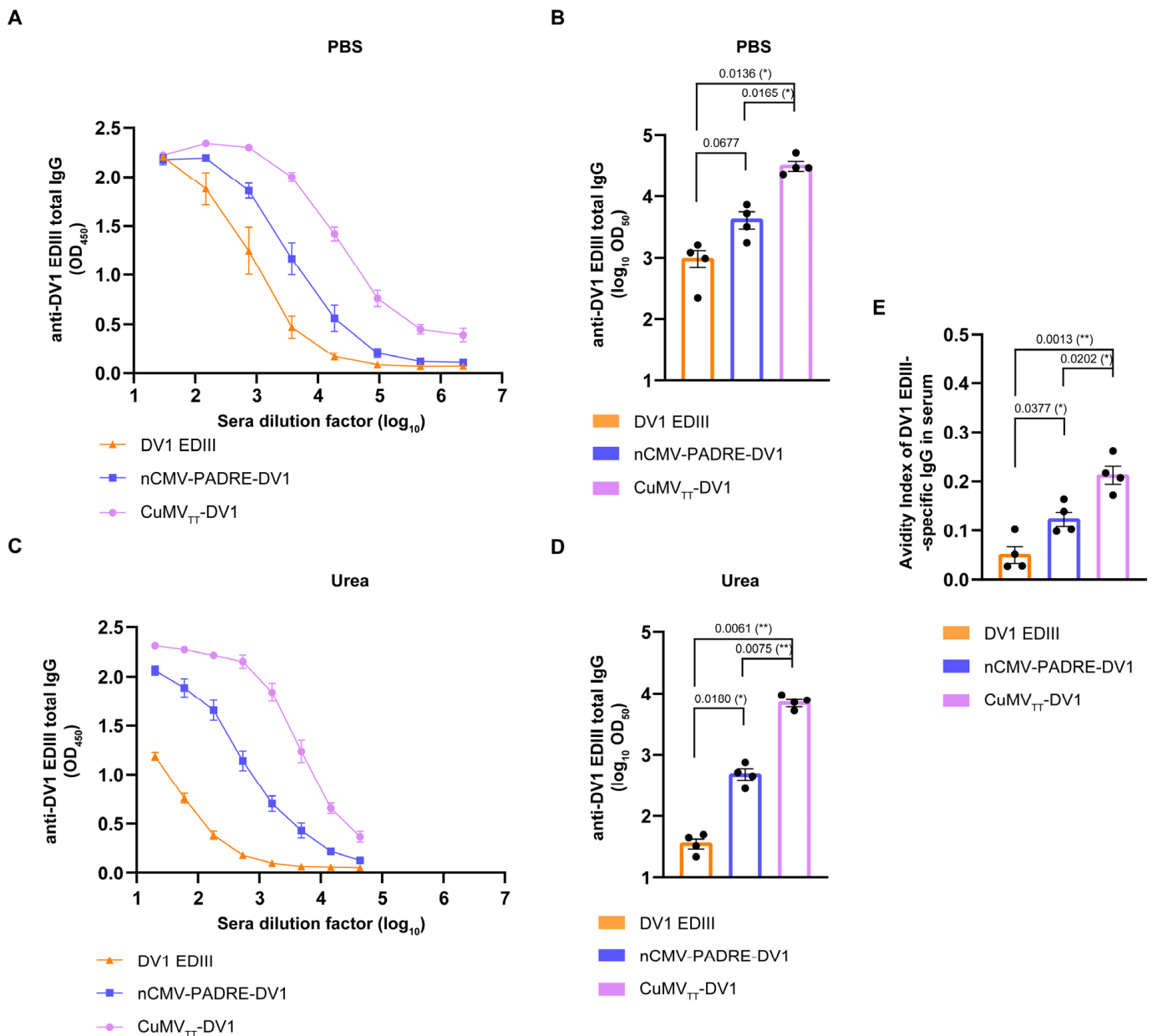
Figure 7. Anti-DV1 EDIII total IgG, high-avidity IgG titers after urea treatment, and avidity index (AI) calculation after vaccination with 30 µg of vaccine variants nCMV-PADRE-DV1, CuMV$_{TT}$-DV1, and DV1 EDIII. (**A**)—Specific IgG titers against DV1 EDIII on Day 35 measured at OD 450 nm; (**B**)—log$_{10}$ OD$_{50}$ values of DV1 EDIII-specific IgG titers shown in A; (**C**)—DV1 EDIII-specific IgG titers on day 35, after three additional washes with 7 M urea, measured at OD 450 nm; (**D**)—log$_{10}$ OD$_{50}$ values of DV1 EDIII-specific IgG titers shown in C; (**E**)—avidity index of DV1 EDIII-specific serum IgG titers shown in B and D. Statistical analysis (mean ± SEM) was conducted using Brown-Forsythe and Welch ANOVA tests. Vaccinated groups, *n* = 4. One representative experiment is shown. A value of $p \leq 0.05$ was considered statistically significant (* $p \leq 0.05$, ** $p \leq 0.01$, *** $p \leq 0.001$, **** $p \leq 0.0001$).
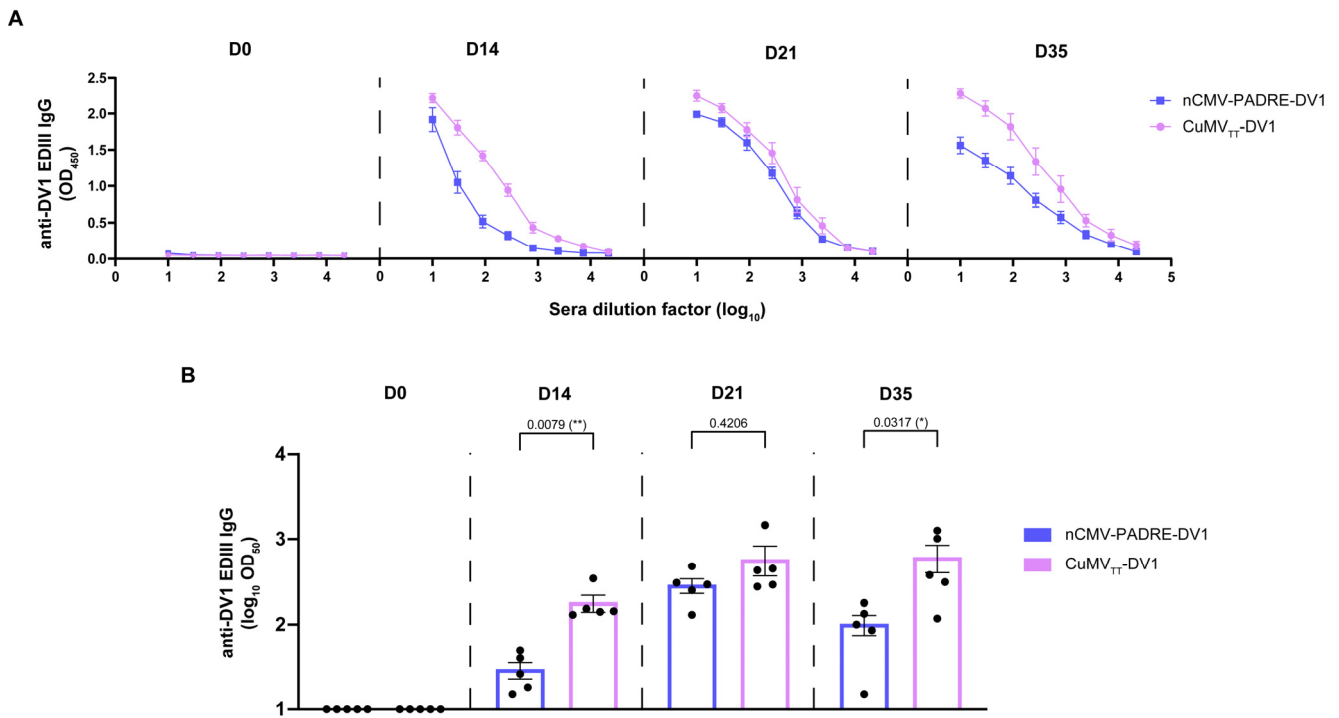
Figure 8. Analysis of anti-DV1 EDIII IgG titers over time following vaccination with nCMV-PADRE-DV1 and CuMV$_{TT}$-DV1 vaccine variants. (**A**)—DV1 EDIII-specific IgG titers measured on days 0, 14, 21, and 35 at OD 450 nm; (**B**)—log$_{10}$ OD$_{50}$ values of DV1 EDIII-specific IgG titers shown in A. Statistical analysis (mean ± SEM) using Welch's *t*-test. Vaccinated groups, *n* = 5. One representative experiment is shown. A value of $p \leq 0.05$ was considered statistically significant (* $p \leq 0.05$, ** $p \leq 0.01$, *** $p \leq 0.001$, **** $p \leq 0.0001$).
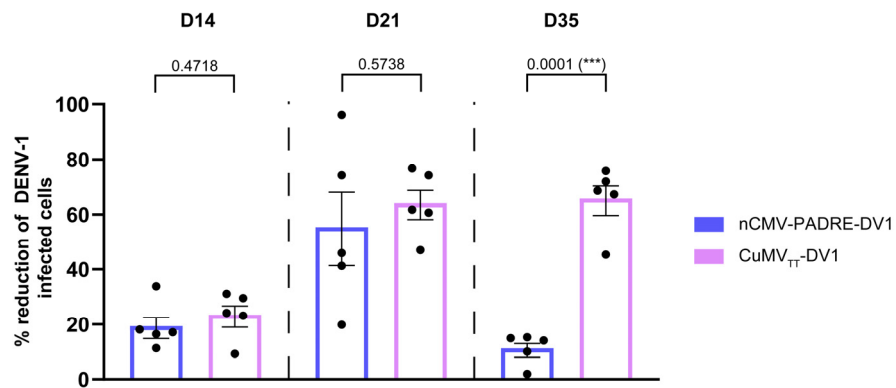

Figure 9. DENV-1 Focus Reduction Virus Neutralization Test (FRNT). FRNT shows the reduction of cells infected with DENV-1 incubated with sera from mice immunized with nCMV-PADRE-DV1 or CuMV$_{TT}$-DV1 collected on days 14, 21, and 35 compared to sera collected on day 0. Statistical analysis (mean ± SEM) using Welch's *t*-test. Vaccinated groups: *n* = 5. A value of $p \leq 0.05$ was considered statistically significant (* $p \leq 0.05$, ** $p \leq 0.01$, *** $p \leq 0.001$, **** $p \leq 0.0001$).

4. Discussion

Several structural elements derived from plant virus CPs were tested and used for multimeric structure formation as "artificial viral nanostructures". By way of example, a 12-mer β-annulus peptide of Sesbania mosaic virus CP with FKFE sequence at the C-terminus self-assembles into a nanosphere of approximately 30 nm in diameter [79], and a 24-mer β-annulus peptide derived from the tomato bushy stunt virus CP spontaneously forms hollow "artificial viral capsids", which can encapsulate anionic dyes, DNAs, quantum

dots, and proteins and can be decorated with recombinant HRP or with a C-terminal His-tag [225]. Beyond plant viruses, peptides from other sources also demonstrated the capacity to self-assemble into nanostructures, serving as versatile tools for designing functional, supramolecular materials that are modular, tunable, and responsive to chemical and physical stimuli [84,209].

The N-terminal fragments of the R domains of CMV CPs form a bundle of six amphipathic helices [166]. This multimerization property could be used as an alternative vaccine platform—the "Immune-tag" [167]. To investigate the utility of those arginine-rich N-terminal domains (nCMVs), two constructs incorporating a model antigen eGFP, one including the additionally fused universal T-cell epitope PADRE [131,140], were initially developed. The use of eGFP was previously tested in the *Brucella abortus* S19 prototype vaccine as an associated diagnostic test to distinguish vaccinated animals from naturally infected with *Brucella* [226]. The incorporation of a universal T-cell epitope was intended to augment immune responses by inducing a strong Th-response against this epitope, which in turn would increase B-cell help [59]. Distinct versions of constructed "Immune-tags" were additionally supplemented with ssRNA to facilitate the formation of a six-helix bundle according to the CMV 3D structure [166] and serve as TLR7/8 stimulators.

Mouse immunization experiments showed a clear trend: the inclusion of additional immunostimulants consistently resulted in higher systemic IgG titers. Notably, the serum anti-eGFP IgG levels elicited by CuMV-eGFP VLPs were substantially higher than those triggered by the nCMV-PADRE-eGFP "Immune-tag", regardless of RNA addition. These findings highlight the importance of a multifaceted approach in vaccine design, demonstrating that optimal immunogenicity relies not only on the inclusion of B-cell [227] and T-cell stimulating epitopes [43,59,151], or TLR ligands such as TLR3 [160,228] and TLR7/8 [160,229,230], but also on the physical properties of the particle/antigen delivery system. Specifically, the size of the particle [5,231–233], its multimerization [1,234], and its repetitiveness [114] play crucial roles in enhancing the immune response.

Building on the results of immunizations with eGFP-carrying "Immune-tags", a dengue vaccine candidate, nCMV-PADRE-DV1, was developed. For this vaccine, DV1 EDIII, containing neutralizing epitopes, was selected as the experimental antigen. The humoral responses in the form of anti-DV1 EDIII IgG were significantly higher in sera collected from mice immunized with a VLP-based vaccine than in those immunized with a nCMV-based linear, multimerized construct. In addition, CuMV$_{TT}$-DV1, following the boost, induced a prolonged and stable neutralizing response while such a response, induced by the oligomeric nCMV-PADRE-DV1 was transient only. The induction of high levels of neutralizing Abs against DENV-1 directly confirms that DV1 EDIII antigen maintains its authentic tertiary and quaternary structures. Given the well-established correlation between neutralizing Ab titers and protection in both humans and mice [235–237], our experimental data confirm the functional efficacy of our vaccine designs, even in the absence of direct DENV challenge data.

The neutralization ratio of DENV-1 can be attributed to several factors that may relate to both the quantity and quality of the elicited Abs. Our observations from the avidity ELISA assay indicate a significant increase in the ratio of high-affinity DV1 EDIII-specific IgG induced by nCMV-PADRE-DV1 compared to "free" DV1 EDIII protein. This underscores the effectiveness of incorporating the described stimulatory elements in enhancing the immunogenicity of the antigen. Importantly, we observed the ability of CuMV$_{TT}$-DV1 to induce the highest ratio of high-affinity DV1 EDIII-specific IgG Abs among all tested vaccine constructs. Enhanced neutralization of DENV-1 by CuMV$_{TT}$-DV1-induced serum post-boost contrasted with low neutralization despite relatively high DV1 EDIII-specific IgG responses observed pre-boost. This might be attributed to the initial Ab repertoire being predominantly composed of low-affinity Abs, which are less effective at DENV-1 neutralization [238,239]. This suggests that not only the quantity but also the quality of the Ab response may be critical for effective neutralization and long-term protection against DENV [240,241].

VLPs closely mimic the natural structure of viruses and present antigens in a repetitive, high-density manner that is optimal for B-cell receptor cross-linking and activation [1–3]. VLPs [242,243] and nanoparticle formulations have also been shown to be efficiently endocytosed by dendritic cells, which, in turn, leads to improved T-cell priming [244]. The design of VLPs/nanoparticles may promote a more balanced Th1/Th2 cell response [242,244], which leads to balanced Ab subclass responses [55,56,59,164]. In the context of generating the dengue vaccine candidates, the versatility of the VLP platforms allows for the exploration of VLPs derived directly from DENV (DENV VLPs) [180,245–247] or the use of other viral CP-based VLPs from sources such as mammalian viruses [182,248], plant viruses [50,51,249], or bacteriophages [77,250,251]. Broad comparative studies across different platforms could provide insight into their respective strengths and limitations in vaccine development, anti-dengue efficacy and safety. Meanwhile, our current study evaluates the impact of immunological cues and nanostructure patterns on the immune response, using the EDIII of DENV-1 as a biologically relevant model antigen.

Insights concerning targeting TLR4 and TLR3 with adjuvants (such as AS04 or NexaVant™, respectively) have been well documented in the literature [252,253]. This study introduces a novel perspective by specifically exploring the potential of targeting TLR7/8 within the framework of VLP-based vaccines. However, the mechanisms by which RNA influences immunogenicity are not yet fully understood. Our recently published study highlights the significant contribution of prokaryotic RNA encapsulated by the VLPs to the VLP-based vaccine's immunogenicity through direct TLR7 and TLR3 engagement in B cells [160,254,255]. Here, we have not observed such a significant effect after supplementation of the "Immune-tags" with exogenous RNA. Moreover, the IgG responses induced by nCMV-based constructs (predominantly IgG1) resemble those triggered by proteins, and anti-viral protein-based vaccines often formulated with aluminum-based adjuvants [256,257]. Several factors may account for the observed differences in immunogenicity between the "Immune-tag"- and VLP-based vaccines: (1) the lack of sufficient doses/booster injections to potentially compensate for deficiencies in TLR 7 signaling and adequately increase the overall quantity of produced IgG Abs [160,255]; (2) the absence of nucleoside modifications characteristic of prokaryotic mRNA [125] within WT CMV CP mRNA obtained by in vitro transcription and supplemented to nCMV, what could impact the immune recognition [258–260]; (3) the insufficient amount of ssRNA [160], particularly lacking in polyU sequences [261,262], which are crucial for effective TLR7 stimulation; (4) suboptimal antigen distribution on the "Immune-tag" surface [116,160], potentially affecting the efficacy of antigen presentation; (5) the lack of dsRNA sequences that stimulate TLR3 [160,263]; (6) RNA degradation by RNases [264,265]; (7) reduced stability of the RNA during storage [266–268], which may be different if packaged within VLPs versus attached in the "free form" to multimers. Despite these challenges, the stimulation of immune responses by RNA needs further investigation, as achieving long-lasting immune responses is crucial for vaccinology. Recent experiences with COVID-19 highlight the complexity of designing effective vaccines [269].

When antigens are genetically fused to VLPs, the vaccine development process requires only single expression and purification steps. However, not all antigens can be effectively incorporated into the VLP structure through genetic fusion due to steric and/or folding issues. On the other hand, chemical conjugation requires a multistep process involving the separate expression and purification of both the VLP and antigen, followed by their conjugation and the final purification of the conjugated product. This prompts the search for alternative vaccine platforms and lead us to develop nCMV-based "Immune-tag" constructs. Such versatile antigen carriers overcome the limitations of direct genetic fusion methods, offering a potentially more cost-effective approach to vaccine design. The fact that the "Immune-tags" do not elicit Abs against the CMV CP provides an opportunity for their application as a booster vaccine after the administration of a first dose of $CuMV_{TT}$ VLP-based vaccine [60,62,63,162,270–272], possibly with a suitable adjuvant. This feature suggests that the "Immune-tag"-based vaccines could be used to enhance and extend the

immune response generated by the initial vaccination without the risk of cross-reactivity or interference with the primary vaccine's antigenic targets [273–276]. The strategy of using "Immune-tag"-based vaccines has the potential to improve vaccination regimens but may also lead to increased cost efficiency in vaccine production [43,54–56,59]. This is particularly relevant when the production of a primary vaccine involves the chemical conjugation of an antigen to a carrier. The "Immune-tag" constructs can be expressed in *E. coli* culture in a single procedure with the same approach as VLPs. The capacity and flexibility of "Immune-tags" allow for the genetic fusion of multiple antigens and the incorporation of various effective immunostimulants while maintaining a simplified vaccine manufacturing process. Hence, VLP/"Immune-tag" combinations may be ideal for use in prime-boost regimens.

Supplementary Materials: The following supporting information can be downloaded at: https://www.mdpi.com/article/10.3390/vaccines12060661/s1, Figure S1: nCMV-eGFP; Figure S2: nCMV-PADRE-eGFP; Figure S3: nCMV-PADRE-DV1; Figure S4: eGFP; Figure S5: DV1 EDIII; Figure S6: nCMV binding to the nucleic acid; Figure S7: Gel shift assays of nCMV-eGFP with distinct nucleic acid species; Figure S8: Analysis of anti-CuMV total IgG titers after vaccination with different vaccine variants; Figure S9: Analysis of anti-eGFP IgG2a subclass titers after vaccination with different vaccine variants.

Author Contributions: J.M.S., I.B. (Irena Barkovska), I.B. (Ina Balke), D.S., M.F.B. and A.Z.: Design of experiments and methodology. J.M.S., I.B. (Irena Barkovska), I.B. (Ina Balke), D.A.R., D.S., A.O., B.M., J.J., J.B., M.F.B. and A.Z.: Acquisition of data, analysis, and interpretation. J.M.S., I.B. (Irena Barkovska), I.B. (Ina Balke), A.O., M.F.B. and A.Z.: Writing, revision, and editing of the manuscript. M.O.M., D.S., B.M., J.J., J.B., M.V., M.F.B. and A.Z.: Technical, material, and tool support. M.O.M., M.V., M.F.B. and A.Z.: Study supervision. All authors have read and agreed to the published version of the manuscript.

Institutional Review Board Statement: All animal-related procedures in this study were approved by either the Animal Protection Ethical Committee of the Latvian Food and Veterinary Service (permission No. 89), and were conducted in compliance with Directive 2010/63/EU as adopted by the national legislation, or the Swiss Cantonal Veterinary Office (license no. BE 70/18).

Informed Consent Statement: Not applicable.

Data Availability Statement: The data supporting the findings of this study are available within the article and supporting materials. The data presented in this study are available upon request.

Conflicts of Interest: M. F. Bachmann is a board member of Saiba AG and holds the patent for CuMV$_{TT}$. J. M. Sobczak and M. O. Mohsen received payments from Saiba AG to work on the development of vaccines against Dengue Fever in the framework of a Eurostars grant as well as against SARS-CoV-2. M. F. Bachmann and M. O. Mohsen are shareholders of Saiba AG.

Abbreviations

2,5-DHAP	2,5-dihydroxyacetophenone
Ab/Abs	antibody/antibodies
AEC	addition of 3-amino-9-ethylcarbazole
APCs	antigen-presenting cells
AI	avidity index
CMV	cucumber mosaic virus
CP	capsid or coat protein
CuMV	cucumber mosaic virus-derived virus-like particles
CuMV$_{TT}$	immunologically optimized cucumber mosaic virus-derived VLPs with incorporated universal Th-cell epitope from tetanus toxin

DENV	dengue virus
DLS	dynamic light scattering
DV1 EDIII	third domain of dengue virus 1 envelope protein
eGFP	enhanced green fluorescent protein
ELISA	enzyme-linked immunosorbent assay
FRNT	focus reduction virus neutralization test
IB	inclusion bodies
MS	mass spectrometry
NAGE	native agarose gel electrophoresis
nCMV	N-terminal fragment of the cucumber mosaic virus capsid protein containing the functional R domain
ON	overnight
PADRE	universal synthetic non-natural Pan DR Epitope
PAMPs	pathogen-associated molecular patterns
PASPs	Pathogen-associated structural patterns
PMSF	phenylmethylsulfonyl fluoride
RT	room temperature
SATA	N-succinimidyl S-acetylthioacetate
s.c.	subcutaneous
SDS-PAGE	sodium dodecyl sulfate-polyacrylamide gel electrophoresis
SMPH	succinimidyl 6-((β-maleimidopropionamido) hexanoate
TEM	transmission electron microscopy
Th	T-cell help
Th cell	T-helper cell
TLR	toll-like receptor
TMB	tetramethylbenzidine
TT	tetanus toxin
VLPs	virus-like particles
WT	wild type

References

1. Feldmann, M.; Easten, A. The relationship between antigenic structure and the requirement for thymus-derived cells in the immune response. *J. Exp. Med.* **1971**, *134*, 103–119. [CrossRef]
2. Bachmann, M.F.; Jennings, G.T. Vaccine delivery: A matter of size, geometry, kinetics, and molecular patterns. *Nat. Rev. Immunol.* **2010**, *10*, 787–796. [CrossRef]
3. Vogel, M.; Bachmann, M.F. Immunogenicity and immunodominance in antibody responses. *Curr. Top. Microbiol. Immunol.* **2020**, *428*, 89–102.
4. Pushko, P.; Pumpens, P.; Grens, E. Development of virus-like particle technology from small highly symmetric to large complex virus-like particle structures. *Intervirology* **2013**, *56*, 141–165. [CrossRef]
5. Zinkhan, S.; Ogrina, A.; Balke, I.; Reseviča, G.; Zeltins, A.; de Brot, S.; Lipp, C.; Chang, X.; Zha, L.; Vogel, M.; et al. The impact of size on particle drainage dynamics and antibody response. *J. Control. Release* **2021**, *331*, 296–308. [CrossRef]
6. Evtushenko, E.A.; Ryabchevskaya, E.M.; Nikitin, N.A.; Atabekov, J.G.; Karpova, O.V. Plant virus particles with various shapes as potential adjuvants. *Sci. Rep.* **2020**, *10*, 10365. [CrossRef]
7. Hilleman, M.R.; Bertland, A.U.; Buynak, E.B.; Lampson, G.P.; McAleer, W.J.; McLean, A.A.; Roehm, R.R.; Tytell, A.A. *Clinical and laboratory studies of HBsAg vaccine*; Vyas, G.N., Cohen, S.N., Schmid, R., Eds.; Franklin Institute Press: Philadelphia, PA, USA, 1978; pp. 525–537.
8. Hilleman, M.R. Yeast recombinant hepatitis B vaccine. *Infection* **1987**, *15*, 3–7. [CrossRef]
9. Mohsen, M.O.; Bachmann, M.F. Virus-like particle vaccinology, from bench to bedside. *Cell. Mol. Immunol.* **2022**, *19*, 993–1011. [CrossRef]
10. Kheirvari, M.; Liu, H.; Tumban, E. Virus-like Particle Vaccines and Platforms for Vaccine Development. *Viruses* **2023**, *15*, 1109. [CrossRef]
11. Schiller, J.T.; Lowy, D.R. Papillomavirus-like particles and HPV vaccine development. *Semin. Cancer Biol.* **1996**, *7*, 373–382. [CrossRef]
12. Worm, H.C.; Wirnsberger, G. Hepatitis E vaccines: Progress and prospects. *Drugs* **2004**, *64*, 1517–1531. [CrossRef]
13. Xia, M.; Farkas, T.; Jiang, X. Norovirus capsid protein expressed in yeast forms virus-like particles and stimulates systemic and mucosal immunity in mice following an oral administration of raw yeast extracts. *J. Med. Virol.* **2007**, *79*, 74–83. [CrossRef]
14. Ross, T.M.; Mahmood, K.; Crevar, C.J.; Schneider-Ohrum, K.; Heaton, P.M.; Bright, R.A. A trivalent virus-like particle vaccine elicits protective immune responses against seasonal influenza strains in mice and ferrets. *PLoS ONE* **2009**, *4*, e6032. [CrossRef]

15. Yang, Y.; Li, X.; Yang, H.; Qian, Y.; Zhang, Y.; Fang, R.; Chen, X. Immunogenicity and virus-like particle formation of rotavirus capsid proteins produced in transgenic plants. *Sci. China Life Sci.* **2011**, *54*, 82–89. [CrossRef]

16. Akahata, W.; Yang, Z.-Y.; Andersen, H.; Sun, S.; Holdaway, H.A.; Kong, W.-P.; Lewis, M.G.; Higgs, S.; Rossmann, M.G.; Rao, S. A virus-like particle vaccine for epidemic Chikungunya virus protects nonhuman primates against infection. *Nat. Med.* **2010**, *16*, 334–338. [CrossRef]

17. Bernstein, D.I.; Sahly, H.M.E.; Keitel, W.A.; Wolff, M.; Simone, G.; Segawa, C.; Wong, S.; Shelly, D.; Young, N.S.; Dempsey, W. Safety and immunogenicity of a candidate parvovirus B19 vaccine. *Vaccine* **2011**, *29*, 7357–7363. [CrossRef]

18. Li, H.Y.; Han, J.F.; Qin, C.F.; Chen, R. Virus-like particles for enterovirus 71 produced from Saccharomyces cerevisiae potently elicits protective immune responses in mice. *Vaccine* **2013**, *31*, 3281–3287. [CrossRef]

19. Zhao, H.; Li, H.Y.; Han, J.F.; Deng, Y.Q.; Li, Y.X.; Zhu, S.Y.; He, Y.L.; Qin, E.D.; Chen, R.; Qin, C.F. Virus-like particles produced in Saccharomyces cerevisiae elicit protective immunity against Coxsackievirus A16 in mice. *Appl. Microbiol. Biotechnol.* **2013**, *97*, 10445–10452. [CrossRef]

20. Chang, L.J.; Dowd, K.A.; Mendoza, F.H.; Saunders, J.G.; Sitar, S.; Plummer, S.H.; Yamshchikov, G.; Sarwar, U.N.; Hu, Z.; Enama, M.E.; et al. Safety and tolerability of chikungunya virus-like particle vaccine in healthy adults: A phase 1 dose-escalation trial. *Lancet* **2014**, *384*, 2046–2052. [CrossRef]

21. Walpita, P.; Cong, Y.; Jahrling, P.B.; Rojas, O.; Postnikova, E.; Yu, S.; Johns, L.; Holbrook, M. A VLP-based vaccine provides complete protection against Nipah virus challenge following multiple-dose or single-dose vaccination schedules in a hamster model. *NPJ Vaccines* **2017**, *2*, 21. [CrossRef]

22. Sunay, M.M.E.; Martins, K.A.O.; Steffens, J.T.; Gregory, M.; Vantongeren, S.A.; Van Hoeven, N.; Garnes, P.G.; Bavari, S. Glucopyranosyl lipid adjuvant enhances immune response to Ebola virus-like particle vaccine in mice. *Vaccine* **2019**, *37*, 3902–3910. [CrossRef]

23. Chang, Y.H.; Chiao, D.J.; Hsu, Y.L.; Lin, C.C.; Wu, H.L.; Shu, P.Y.; Chang, S.F.; Chang, J.H.; Kuo, S.C. Mosquito cell-derived Japanese encephalitis virus-like particles induce specific humoral and cellular immune responses in mice. *Viruses* **2020**, *12*, 336. [CrossRef]

24. Vang, L.; Morello, C.S.; Mendy, J.; Thompson, D.; Manayani, D.; Guenther, B.; Julander, J.; Sanford, D.; Jain, A.; Patel, A.; et al. Zika virus-like particle vaccine protects AG129 mice and rhesus macaques against Zika virus. *PLoS Negl. Trop. Dis.* **2021**, *15*, e0009195. [CrossRef]

25. Ward, B.J.; Gobeil, P.; Séguin, A.; Atkins, J.; Boulay, I.; Charbonneau, P.Y.; Couture, M.; D'Aoust, M.A.; Dhaliwall, J.; Finkle, C. Phase 1 randomized trial of a plant-derived virus-like particle vaccine for COVID-19. *Nat. Med.* **2021**, *27*, 1071–1078. [CrossRef]

26. Brown, C.S.; Welling-Wester, S.; Feijlbrief, M.; Van Lent, J.W.; Spaan, W.J. Chimeric parvovirus B19 capsids for the presentation of foreign epitopes. *Virology* **1994**, *198*, 477–488. [CrossRef]

27. Tan, M.; Xia, M.; Huang, P.; Wang, L.; Zhong, W.; McNeal, M.; Wei, C.; Jiang, X. Norovirus P particle as a platform for antigen presentation. *Procedia Vaccinol.* **2011**, *4*, 19–26. [CrossRef]

28. Jiang, L.; Fan, R.; Sun, S.; Fan, P.; Su, W.; Zhou, Y.; Gao, F.; Xu, F.; Kong, W.; Jiang, C. A new EV71 VP3 epitope in norovirus P particle vector displays neutralizing activity and protection in vivo in mice. *Vaccine* **2015**, *33*, 6596–6603. [CrossRef]

29. Pascual, E.; Mata, C.P.; Gómez-Blanco, J.; Moreno, N.; Bárcena, J.; Blanco, E.; Rodríguez-Frandsen, A.; Nieto, A.; Carrascosa, J.L.; Castón, J.R. Structural basis for the development of avian virus capsids that display influenza virus proteins and induce protective immunity. *J. Virol.* **2015**, *89*, 2563–2574. [CrossRef]

30. Wang, C.; Zheng, X.; Gai, W.; Wong, G.; Wang, H.; Jin, H.; Feng, N.; Zhao, Y.; Zhang, W.; Li, N. Novel chimeric virus-like particles vaccine displaying MERS-CoV receptor-binding domain induce specific humoral and cellular immune response in mice. *Antivir. Res.* **2017**, *140*, 55–61. [CrossRef]

31. Czarnota, A.; Offersgaard, A.; Pihl, A.F.; Prentoe, J.; Bukh, J.; Gottwein, J.M.; Bieńkowska-Szewczyk, K.; Grzyb, K. Specific Antibodies Induced by Immunization with Hepatitis B Virus-Like Particles Carrying Hepatitis C Virus Envelope Glycoprotein 2 Epitopes Show Differential Neutralization Efficiency. *Vaccines* **2020**, *8*, 294. [CrossRef]

32. Kotiw, M.; Johnson, M.; Pandey, M.; Fry, S.; Hazell, S.L.; Netter, H.J.; Good, M.F.; Olive, C. Immunological response to parenteral vaccination with recombinant hepatitis B virus surface antigen virus-like particles expressing Helicobacter pylori KatA epitopes in a murine H. pylori challenge model. *Clin. Vaccine Immunol.* **2012**, *19*, 268–276. [CrossRef]

33. Rashidijahanabad, Z.; Kelly, M.; Kamruzzaman, M.; Qadri, F.; Bhuiyan, T.R.; McFall-Boegeman, H.; Wu, D.; Piszczek, G.; Xu, P.; Ryan, E.T.; et al. Virus-like Particle Display of Vibrio cholerae O-Specific Polysaccharide as a Potential Vaccine against Cholera. *ACS Infect. Dis.* **2022**, *8*, 574–583. [CrossRef]

34. Rutgers, T.; Gordon, O.M.; Gathoye, A.M.; Hockmeyer, W.T.; De Wilde, M.; Rosenberg, M. Hepatitis B surface antigen as a carrier matrix for the repetitive epitope of the circumsporozoite protein of Plasmodium falciparum. *Biotechnology* **1988**, *6*, 1065–1070. [CrossRef]

35. Lee, D.H.; Lee, S.H.; Kim, A.R.; Quan, F.S. Virus-Like Nanoparticle Vaccine Confers Protection against Toxoplasma gondii. *PLoS ONE* **2016**, *11*, e0161231. [CrossRef]

36. Collins, K.A.; Snaith, R.; Cottingham, M.G.; Gilbert, S.C.; Hill, A.V.S. Enhancing protective immunity to malaria with a highly immunogenic virus-like particle vaccine. *Sci. Rep.* **2017**, *7*, 46621. [CrossRef]

37. Cecílio, P.; Pérez-Cabezas, B.; Fernández, L.; Moreno, J.; Carrillo, E.; Requena, J.M.; Fichera, E.; Reed, S.G.; Coler, R.N.; Kamhawi, S.; et al. Pre-clinical antigenicity studies of an innovative multivalent vaccine for human visceral leishmaniasis. *PLoS Negl. Trop. Dis.* **2017**, *11*, e0005951. [CrossRef]

38. Moura, A.P.V.; Santos, L.C.B.; Brito, C.R.N.; Valencia, E.; Junqueira, C.; Filho, A.A.P.; Sant'Anna, M.R.V.; Gontijo, N.F.; Bartholomeu, D.C.; Fujiwara, R.T.; et al. Virus-like Particle Display of the α-Gal Carbohydrate for Vaccination against Leishmania Infection. *ACS Cent. Sci.* **2017**, *3*, 1026–1031. [CrossRef]

39. Chackerian, B.; Lowy, D.R.; Schiller, J.T. Conjugation of a self-antigen to papillomavirus-like particles allows for efficient induction of protective autoantibodies. *J. Clin. Investig.* **2001**, *108*, 415–423. [CrossRef]

40. Di Bonito, P.; Grasso, F.; Mochi, S.; Petrone, L.; Fanales-Belasio, E.; Mei, A.; Cesolini, A.; Laconi, G.; Conrad, H.; Bernhard, H.; et al. Anti-tumor CD8+ T cell immunity elicited by HIV-1-based virus-like particles incorporating HPV-16 E7 protein. *Virology* **2009**, *395*, 45–55. [CrossRef]

41. Cubas, R.; Zhang, S.; Li, M.; Chen, C.; Yao, Q. Chimeric Trop2 virus-like particles: A potential immunotherapeutic approach against pancreatic cancer. *J. Immunother.* **2011**, *34*, 251–263. [CrossRef]

42. Spohn, G.; Arenas-Ramirez, N.; Bouchaud, G.; Boyman, O. Endogenous polyclonal anti-IL-1 antibody responses potentiate IL-1 activity during pathogenic inflammation. *J. Allergy Clin. Immunol.* **2017**, *139*, 1957–1965.e3. [CrossRef]

43. Zeltins, A.; West, J.; Zabel, F.; El Turabi, A.; Balke, I.; Haas, S.; Maudrich, M.; Storni, F.; Engeroff, P.; Jennings, G.T.; et al. Incorporation of tetanus-epitope into virus-like particles achieves vaccine responses even in older recipients in models of psoriasis, alzheimer's and cat allergy. *NPJ Vaccines* **2017**, *2*, 30. [CrossRef]

44. Palladini, A.; Thrane, S.; Janitzek, C.M.; Pihl, J.; Clemmensen, S.B.; de Jongh, W.A.; Clausen, T.M.; Nicoletti, G.; Landuzzi, L.; Penichet, M.L.; et al. Virus-like particle display of HER2 induces potent anti-cancer responses. *Oncoimmunology* **2018**, *7*, e1408749. [CrossRef]

45. Schumacher, J.; Bacic, T.; Staritzbichler, R.; Daneschdar, M.; Klamp, T.; Arnold, P.; Jägle, S.; Türeci, Ö.; Markl, J.; Sahin, U. Enhanced stability of a chimeric hepatitis B core antigen virus-like-particle (HBcAg-VLP) by a C-terminal linker-hexahistidine-peptide. *J. Nanobiotechnol.* **2018**, *16*, 39. [CrossRef]

46. Storni, F.; Zeltins, A.; Balke, I.; Heath, M.D.; Kramer, M.F.; Skinner, M.A.; Zha, L.; Roesti, E.; Engeroff, P.; Muri, L.; et al. Vaccine against peanut allergy based on engineered virus-like particles displaying single major peanut allergens. *J. Allergy Clin. Immunol.* **2020**, *145*, 1240–1253.e3. [CrossRef]

47. Cheng, K.; Du, T.; Li, Y.; Qi, Y.; Min, H.; Wang, Y.; Zhang, Q.; Wang, C.; Zhou, Y.; Li, L.; et al. Dual-Antigen-Loaded Hepatitis B Virus Core Antigen Virus-like Particles Stimulate Efficient Immunotherapy against Melanoma. *ACS Appl. Mater. Interfaces* **2020**, *12*, 53682–53690. [CrossRef]

48. Rolih, V.; Caldeira, J.; Bolli, E.; Salameh, A.; Conti, L.; Barutello, G.; Riccardo, F.; Magri, J.; Lamolinara, A.; Parra, K.; et al. Development of a VLP-Based Vaccine Displaying an xCT Extracellular Domain for the Treatment of Metastatic Breast Cancer. *Cancers* **2020**, *12*, 1492. [CrossRef]

49. Klimek, L.; Kundig, T.; Kramer, M.F.; Guethoff, S.; Jensen-Jarolim, E.; Schmidt-Weber, C.B.; Palomares, O.; Mohsen, M.O.; Jakob, T.; Bachmann, M. Virus-like particles (VLP) in prophylaxis and immunotherapy of allergic diseases. *Allergo J. Int.* **2018**, *27*, 245–255. [CrossRef]

50. Balke, I.; Zeltins, A. Use of plant viruses and virus-like particles for the creation of novel vaccines. *Adv. Drug Deliv. Rev.* **2019**, *145*, 119–129. [CrossRef]

51. Balke, I.; Zeltins, A. Recent advances in the use of plant virus-like particles as vaccines. *Viruses* **2020**, *12*, 270. [CrossRef]

52. Mohsen, M.O.; Speiser, D.E.; Knuth, A.; Bachmann, M.F. Virus-like particles for vaccination against cancer. *Wiley Interdiscip. Rev. Nanomed. Nanobiotechnol.* **2020**, *12*, e1579. [CrossRef]

53. Liu, X.; Chang, X.; Rothen, D.; Derveni, M.; Krenger, P.; Roongta, S.; Wright, E.; Vogel, M.; Tars, K.; Mohsen, M.O.; et al. AP205 VLPs Based on Dimerized Capsid Proteins Accommodate RBM Domain of SARS-CoV-2 and Serve as an Attractive Vaccine Candidate. *Vaccines* **2021**, *9*, 403. [CrossRef]

54. Chang, X.; Zeltins, A.; Mohsen, M.O.; Gharailoo, Z.; Zha, L.; Liu, X.; Walton, S.; Vogel, M.; Bachmann, M.F. A novel double mosaic virus-like particle-based vaccine against SARS-CoV-2 incorporates both receptor binding motif (RBM) and fusion domain. *Vaccines* **2021**, *9*, 1287. [CrossRef] [PubMed]

55. Mohsen, M.O.; Rothen, D.; Balke, I.; Martina, B.; Zeltina, V.; Inchakalody, V.; Gharailoo, Z.; Nasrallah, G.; Dermime, S.; Tars, K. Neutralization of MERS coronavirus through a scalable nanoparticle vaccine. *NPJ Vaccines* **2021**, *6*, 107. [CrossRef] [PubMed]

56. Mohsen, M.O.; Balke, I.; Zinkhan, S.; Zeltina, V.; Liu, X.; Chang, X.; Krenger, P.S.; Plattner, K.; Gharailoo, Z.; Vogt, A.C.S.; et al. A scalable and highly immunogenic virus-like particle-based vaccine against SARS-CoV-2. *Allergy* **2022**, *77*, 243–257. [CrossRef] [PubMed]

57. Ogrina, A.; Skrastina, D.; Balke, I.; Kalnciema, I.; Jansons, J.; Bachmann, M.F.; Zeltins, A. Comparison of bacterial expression systems based on potato virus Y-like particles for vaccine generation. *Vaccines* **2022**, *10*, 485. [CrossRef]

58. Ogrina, A.; Balke, I.; Kalnciema, I.; Skrastina, D.; Jansons, J.; Bachmann, M.F.; Zeltins, A. Bacterial expression systems based on Tymovirus-like particles for the presentation of vaccine antigens. *Front. Microbiol.* **2023**, *14*, 1154990. [CrossRef] [PubMed]

59. Sobczak, J.M.; Krenger, P.S.; Storni, F.; Mohsen, M.O.; Balke, I.; Reseviča, G.; Heath, M.D.; Carreno Velazquez, T.L.; Kramer, M.F.; Scott, C.J.W.; et al. The next generation virus-like particle platform for the treatment of peanut allergy. *Allergy* **2023**, *78*, 1980–1996. [CrossRef]

60. Cabral-Miranda, G.; Lim, S.M.; Mohsen, M.O.; Pobelov, I.V.; Roesti, E.S.; Heath, M.D.; Skinner, M.A.; Kramer, M.F.; Martina, B.E.E.; Bachmann, M.F. Zika virus-derived E-DIII protein displayed on immunologically optimized VLPs induces neutralizing antibodies without causing enhancement of dengue virus infection. *Vaccines* **2019**, *7*, 72. [CrossRef]

61. Mohsen, M.O.; Heath, M.D.; Cabral-Miranda, G.; Lipp, C.; Zeltins, A.; Sande, M.; Stein, J.V.; Riether, C.; Roesti, E.; Zha, L.; et al. Vaccination with nanoparticles combined with micro-adjuvants protects against cancer. *J. Immunother. Cancer* **2019**, *7*, 114. [CrossRef]

62. Thoms, F.; Jennings, G.T.; Maudrich, M.; Vogel, M.; Haas, S.; Zeltins, A.; Hofmann-Lehmann, R.; Riond, B.; Grossmann, J.; Hunziker, P. Immunization of cats to induce neutralizing antibodies against Fel d 1, the major feline allergen in human subjects. *J. Allergy Clin. Immunol.* **2019**, *144*, 193–203. [CrossRef] [PubMed]

63. Olomski, F.; Fettelschoss, V.; Jonsdottir, S.; Birkmann, K.; Thoms, F.; Marti, E.; Bachmann, M.F.; Kundig, T.M.; Fettelschoss-Gabriel, A. Interleukin 31 in insect bite hypersensitivity—Alleviating clinical symptoms by active vaccination against itch. *Allergy* **2020**, *75*, 862–871. [CrossRef] [PubMed]

64. Brune, K.D.; Liekniņa, I.; Sutov, G.; Morris, A.R.; Jovicevic, D.; Kalniņš, G.; Kazāks, A.; Kluga, R.; Kastaljana, S.; Zajakina, A.; et al. N-Terminal Modification of Gly-His-Tagged Proteins with Azidogluconolactone. *Chembiochem* **2021**, *22*, 3199–3207. [CrossRef] [PubMed]

65. Zha, L.; Chang, X.; Zhao, H.; Mohsen, M.O.; Hong, L.; Zhou, Y.; Chen, H.; Liu, X.; Zhang, J.; Li, D.; et al. Development of a Vaccine against SARS-CoV-2 Based on the Receptor-Binding Domain Displayed on Virus-Like Particles. *Vaccines* **2021**, *9*, 395. [CrossRef]

66. Brune, K.D.; Leneghan, D.B.; Brian, I.J.; Ishizuka, A.S.; Bachmann, M.F.; Draper, S.J.; Biswas, S.; Howarth, M. Plug-and-display: Decoration of virus-like particles via isopeptide bonds for modular immunization. *Sci. Rep.* **2016**, *6*, 19234. [CrossRef] [PubMed]

67. Thérien, A.; Bédard, M.; Carignan, D.; Rioux, G.; Gauthier-Landry, L.; Laliberté-Gagné, M.; Bolduc, M.; Savard, P.; Leclerc, D. A versatile papaya mosaic virus (PapMV) vaccine platform based on sortase-mediated antigen coupling. *J. Nanobiotechnol.* **2017**, *15*, 54. [CrossRef] [PubMed]

68. Andersson, A.M.C.; Buldun, C.M.; Pattinson, D.J.; Draper, S.J.; Howarth, M. Snoopligase peptide-peptide conjugation enables modular vaccine assembly. *Sci. Rep.* **2019**, *9*, 4625. [CrossRef] [PubMed]

69. Cohen, A.A.; Yang, Z.; Gnanapragasam, P.N.P.; Ou, S.; Dam, K.A.; Wang, H.; Bjorkman, P.J. Construction, characterization, and immunization of nanoparticles that display a diverse array of influenza HA trimers. *PLoS ONE* **2021**, *16*, e0247963. [CrossRef]

70. Pejawar-Gaddy, S.; Rajawat, Y.; Hilioti, Z.; Xue, J.; Gaddy, D.F.; Finn, O.J.; Viscidi, R.P.; Bossis, I. Generation of a tumor vaccine candidate based on conjugation of a MUC1 peptide to polyionic papillomavirus virus-like particles. *Cancer Immunol. Immunother.* **2010**, *59*, 1685–1696. [CrossRef]

71. van Eldijk, M.B.; Wang, J.C.; Minten, I.J.; Li, C.; Zlotnick, A.; Nolte, R.J.; Cornelissen, J.J.; van Hest, J.C. Designing two self-assembly mechanisms into one viral capsid protein. *J. Am. Chem. Soc.* **2012**, *134*, 18506–18509. [CrossRef]

72. Trifonova, E.A.; Zenin, V.A.; Nikitin, N.A.; Yurkova, M.S.; Ryabchevskaya, E.M.; Putlyaev, E.V.; Donchenko, E.K.; Kondakova, O.A.; Fedorov, A.N.; Atabekov, J.G. Study of rubella candidate vaccine based on a structurally modified plant virus. *Antivir. Res.* **2017**, *144*, 27–33. [CrossRef]

73. Zapata-Cuellar, L.; Gaona-Bernal, J.; Manuel-Cabrera, C.A.; Martínez-Velázquez, M.; Sánchez-Hernández, C.; Elizondo-Quiroga, D.; Camacho-Villegas, T.A.; Gutiérrez-Ortega, A. Development of a platform for noncovalent coupling of full antigens to tobacco etch virus-like particles by means of coiled-coil oligomerization motifs. *Molecules* **2021**, *26*, 4436. [CrossRef]

74. Choi, B.; Kim, H.; Choi, H.; Kang, S. Protein cage nanoparticles as delivery nanoplatforms. *Adv. Exp. Med. Biol.* **2018**, *1064*, 27–43.

75. Nooraei, S.; Bahrulolum, H.; Hoseini, Z.S.; Katalani, C.; Hajizade, A.; Easton, A.J.; Ahmadian, G. Virus-like particles: Preparation, immunogenicity and their roles as nanovaccines and drug nanocarriers. *J. Nanobiotechnol.* **2021**, *19*, 59. [CrossRef]

76. Hadj Hassine, I.; Ben M'hadheb, M.; Almalki, M.A.; Gharbi, J. Virus-like particles as powerful vaccination strategy against human viruses. *Rev. Med. Virol.* **2024**, *34*, e2498. [CrossRef] [PubMed]

77. Tumban, E. Bacteriophage virus-like particles: Platforms for vaccine design. *Methods Mol. Biol.* **2024**, *2738*, 411–423. [PubMed]

78. Matsuura, K.; Watanabe, K.; Matsuzaki, T.; Sakurai, K.; Kimizuka, N. Self-assembled synthetic viral capsids from a 24-mer viral peptide fragment. *Angew. Chem. Int. Ed.* **2010**, *49*, 9662–9665. [CrossRef] [PubMed]

79. Matsuura, K.; Mizuguchi, Y.; Kimizuka, N. Peptide nanospheres self-assembled from a modified β-annulus peptide of sesbania mosaic virus. *Biopolymers* **2016**, *106*, 470–475. [CrossRef] [PubMed]

80. Lainšček, D.; Fink, T.; Forstnerič, V.; Hafner-Bratkovič, I.; Orehek, S.; Strmšek, Ž.; Manček-Keber, M.; Pečan, P.; Esih, H.; Malenšek, Š.; et al. A nanoscaffolded spike-rbd vaccine provides protection against sars-cov-2 with minimal anti-scaffold response. *Vaccines* **2021**, *9*, 431. [CrossRef]

81. Han, J.A.; Kang, Y.J.; Shin, C.; Ra, J.S.; Shin, H.H.; Hong, S.Y.; Do, Y.; Kang, S. Ferritin protein cage nanoparticles as versatile antigen delivery nanoplatforms for dendritic cell (DC)-based vaccine development. *Nanomedicine* **2014**, *10*, 561–569. [CrossRef]

82. Khoshnejad, M.; Parhiz, H.; Shuvaev, V.V.; Dmochowski, I.J.; Muzykantov, V.R. Ferritin-based drug delivery systems: Hybrid nanocarriers for vascular immunotargeting. *J. Control. Release* **2018**, *282*, 13–24. [CrossRef] [PubMed]

83. Lee, N.K.; Cho, S.; Kim, I.S. Ferritin—A multifaceted protein scaffold for biotherapeutics. *Exp. Mol. Med.* **2022**, *54*, 1652–1657. [CrossRef] [PubMed]

84. Obozina, A.S.; Komedchikova, E.N.; Kolesnikova, O.A.; Iureva, A.M.; Kovalenko, V.L.; Zavalko, F.A.; Rozhnikova, T.V.; Tereshina, E.D.; Mochalova, E.N.; Shipunova, V.O. Genetically encoded self-assembling protein nanoparticles for the targeted delivery in vitro and in vivo. *Pharmaceutics* **2023**, *15*, 231. [CrossRef] [PubMed]

85. Reutovich, A.A.; Srivastava, A.K.; Arosio, P.; Bou-Abdallah, F. Ferritin nanocages as efficient nanocarriers and promising platforms for COVID-19 and other vaccines development. *Biochim. Biophys. Acta Gen. Subj.* **2023**, *1867*, 130288. [CrossRef]

86. Moon, H.; Lee, J.; Min, J.; Kang, S. Developing genetically engineered encapsulin protein cage nanoparticles as a targeted delivery nanoplatform. *Biomacromolecules* **2014**, *15*, 3794–3801. [CrossRef] [PubMed]

87. Moon, H.; Lee, J.; Kim, H.; Heo, S.; Min, J.; Kang, S. Genetically engineering encapsulin protein cage nanoparticle as a SCC-7 cell targeting optical nanoprobe. *Biomater. Res.* **2014**, *18*, 21. [CrossRef]

88. Choi, B.; Moon, H.; Hong, S.J.; Shin, C.; Do, Y.; Ryu, S.; Kang, S. Effective delivery of antigen-encapsulin nanoparticle fusions to dendritic cells leads to antigen-specific cytotoxic T cell activation and tumor rejection. *ACS Nano* **2016**, *10*, 7339–7350. [CrossRef]

89. Van de Steen, A.; Khalife, R.; Colant, N.; Khan, H.M.; Deveikis, M.; Charalambous, S.; Robinson, C.M.; Dabas, R.; Esteban Serna, S.; Catana, D.A.; et al. Bioengineering bacterial encapsulin nanocompartments as targeted drug delivery system. *Synth. Syst. Biotechnol.* **2021**, *6*, 231–241. [CrossRef] [PubMed]

90. Azuma, Y.; Edwardson, T.G.W.; Hilvert, D. Tailoring lumazine synthase assemblies for bionanotechnology. *Chem. Soc. Rev.* **2018**, *47*, 3543–3557. [CrossRef]

91. Kang, Y.-F.; Zhang, X.; Yu, X.-H.; Zheng, Q.; Liu, Z.; Li, J.-P.; Sun, C.; Kong, X.-W.; Zhu, Q.-Y.; Chen, H.-W.; et al. Immunization with a self-assembled nanoparticle vaccine elicits potent neutralizing antibody responses against EBV infection. *Nano Lett.* **2021**, *21*, 2476–2486. [CrossRef]

92. Malonis, R.J.; Georgiev, G.I.; Haslwanter, D.; VanBlargan, L.A.; Fallon, G.; Vergnolle, O.; Cahill, S.M.; Harris, R.; Cowburn, D.; Chandran, K.; et al. A Powassan virus domain III nanoparticle immunogen elicits neutralizing and protective antibodies in mice. *PLoS Pathog.* **2022**, *18*, e1010573. [CrossRef]

93. Ulbrich, K.; Hekmatara, T.; Herbert, E.; Kreuter, J. Transferrin- and transferrin-receptor-antibody-modified nanoparticles enable drug delivery across the blood-brain barrier (BBB). *Eur. J. Pharm. Biopharm.* **2009**, *71*, 251–256. [CrossRef]

94. Ferris, D.P.; Lu, J.; Gothard, C.; Yanes, R.; Thomas, C.R.; Olsen, J.-C.; Stoddart, J.F.; Tamanoi, F.; Zink, J.I. Synthesis of biomolecule-modified mesoporous silica nanoparticles for targeted hydrophobic drug delivery to cancer cells. *Small* **2011**, *7*, 1816–1826. [CrossRef] [PubMed]

95. Ramalho, M.J.; Bravo, M.; Loureiro, J.A.; Lima, J.; Pereira, M.C. Transferrin-modified nanoparticles for targeted delivery of asiatic acid to glioblastoma cells. *Life Sci.* **2022**, *296*, 120435. [CrossRef] [PubMed]

96. Golla, K.; Cherukuvada, B.; Ahmed, F.; Kondapi, A.K. Efficacy, safety and anticancer activity of protein nanoparticle-based delivery of doxorubicin through intravenous administration in rats. *PLoS ONE* **2012**, *7*, e51960. [CrossRef]

97. Desoize, B.; Jardillier, J.C.; Kanoun, K.; Guerin, D.; Levy, M.C. In-vitro cytotoxic activity of cross-linked protein microcapsules. *J. Pharm. Pharmacol.* **1986**, *38*, 8–13. [CrossRef] [PubMed]

98. Chen, Y.; Willmott, N.; Anderson, J.; Florence, A.T. Comparison of albumin and casein microspheres as a carrier for doxorubicin. *J. Pharm. Pharmacol.* **1987**, *39*, 978–985. [CrossRef] [PubMed]

99. Chen, L.; Wei, J.; An, M.; Zhang, L.; Lin, S.; Shu, G.; Yuan, Z.; Lin, J.; Peng, G.; Liang, X.; et al. Casein nanoparticles as oral delivery carriers of mequindox for the improved bioavailability. *Colloids Surf. B Biointerfaces* **2020**, *195*, 111221. [CrossRef]

100. Caivano, A.; Doria-Rose, N.A.; Buelow, B.; Sartorius, R.; Trovato, M.; D'Apice, L.; Domingo, G.J.; Sutton, W.F.; Haigwood, N.L.; De Berardinis, P. HIV-1 gag p17 presented as virus-like particles on the E2 scaffold from Geobacillus stearothermophilus induces sustained humoral and cellular immune responses in the absence of IFNγ production by CD4+ T cells. *Virology* **2010**, *407*, 296–305. [CrossRef]

101. Jaworski, J.P.; Krebs, S.J.; Trovato, M.; Kovarik, D.N.; Brower, Z.; Sutton, W.F.; Waagmeester, G.; Sartorius, R.; D'Apice, L.; Caivano, A.; et al. Co-immunization with multimeric scaffolds and DNA rapidly induces potent autologous HIV-1 neutralizing antibodies and CD8+ T cells. *PLoS ONE* **2012**, *7*, e31464. [CrossRef]

102. Molino, N.M.; Neek, M.; Tucker, J.A.; Nelson, E.L.; Wang, S.W. Viral-mimicking protein nanoparticle vaccine for eliciting anti-tumor responses. *Biomaterials* **2016**, *86*, 83–91. [CrossRef] [PubMed]

103. Melchers, M.; Matthews, K.; de Vries, R.P.; Eggink, D.; van Montfort, T.; Bontjer, I.; van de Sandt, C.; David, K.; Berkhout, B.; Moore, J.P.; et al. A stabilized HIV-1 envelope glycoprotein trimer fused to CD40 ligand targets and activates dendritic cells. *Retrovirology* **2011**, *8*, 48. [CrossRef] [PubMed]

104. Sliepen, K.; van Montfort, T.; Melchers, M.; Isik, G.; Sanders, R.W. Immunosilencing a highly immunogenic protein trimerization domain. *J. Biol. Chem.* **2015**, *290*, 7436–7442. [CrossRef] [PubMed]

105. Yan, Y.; Hu, K.; Deng, X.; Guan, X.; Luo, S.; Tong, L.; Du, T.; Fu, M.; Zhang, M.; Liu, Y.; et al. Immunization with HSV-2 gB-CCL19 fusion constructs protects mice against lethal vaginal challenge. *J. Immunol.* **2015**, *195*, 329–338. [CrossRef] [PubMed]

106. Stewart-Jones, G.B.E.; Thomas, P.V.; Chen, M.; Druz, A.; Joyce, M.G.; Kong, W.-P.; Sastry, M.; Soto, C.; Yang, Y.; Zhang, B.; et al. A cysteine zipper stabilizes a pre-fusion F glycoprotein vaccine for respiratory syncytial virus. *PLoS ONE* **2015**, *10*, e0128779. [CrossRef] [PubMed]

107. Gómez-González, J.; Peña, D.G.; Barka, G.; Sciortino, G.; Maréchal, J.-D.; Vázquez López, M.; Vázquez, M.E. Directed self-assembly of trimeric DNA-binding chiral miniprotein helicates. *Front. Chem.* **2018**, *6*, 520. [CrossRef] [PubMed]

108. Kobayashi, N.; Yanase, K.; Sato, T.; Unzai, S.; Hecht, M.H.; Arai, R. Self-assembling nano-architectures created from a protein nano-building block using an intermolecularly folded dimeric de novo protein. *J. Am. Chem. Soc.* **2015**, *137*, 11285–11293. [CrossRef]

109. Kobayashi, N.; Arai, R. Protein cages and nanostructures constructed from protein nanobuilding blocks. *Methods Mol. Biol.* **2023**, *2671*, 79–94. [PubMed]
110. Wang, L.; Prozorov, T.; Palo, P.E.; Liu, X.; Vaknin, D.; Prozorov, R.; Mallapragada, S.; Nilsen-Hamilton, M. Self-assembly and biphasic iron-binding characteristics of mms6, a bacterial protein that promotes the formation of superparamagnetic magnetite nanoparticles of uniform size and shape. *Biomacromolecules* **2012**, *13*, 98–105. [CrossRef]
111. Kotelnikova, P.A.; Shipunova, V.O.; Aghayeva, U.F.; Stremovskiy, O.A.; Nikitin, M.P.; Novikov, I.A.; Schulga, A.A.; Deyev, S.M.; Petrov, R.V. Synthesis of magnetic nanoparticles stabilized by magnetite-binding protein for targeted delivery to cancer cells. *Dokl. Biochem. Biophys.* **2018**, *481*, 198–200. [CrossRef]
112. Shipunova, V.O.; Kotelnikova, P.A.; Aghayeva, U.F.; Stremovskiy, O.A.; Novikov, I.A.; Schulga, A.A.; Nikitin, M.P.; Deyev, S.M. Self-assembling nanoparticles biofunctionalized with magnetite-binding protein for the targeted delivery to HER2/neu overexpressing cancer cells. *J. Magn. Magn. Mater.* **2019**, *469*, 450–455. [CrossRef]
113. Clem, A.S. Fundamentals of vaccine immunology. *J. Glob. Infect. Dis.* **2011**, *3*, 73–78. [CrossRef]
114. Mohsen, M.O.; Augusto, G.; Bachmann, M.F. The 3Ds in virus-like particle based-vaccines: "Design, Delivery and Dynamics". *Immunol. Rev.* **2020**, *296*, 155–168. [CrossRef] [PubMed]
115. Ochsenbein, A.F.; Fehr, T.; Lutz, C.; Suter, M.; Brombacher, F.; Hengartner, H.; Zinkernagel, R.M. Control of early viral and bacterial distribution and disease by natural antibodies. *Science* **1999**, *286*, 2156–2159. [CrossRef] [PubMed]
116. Vogelstein, B.; Dintzis, R.Z.; Dintzis, H.M. Specific cellular stimulation in the primary immune response: A quantized model. *Proc. Natl. Acad. Sci. USA* **1982**, *79*, 395–399. [CrossRef] [PubMed]
117. Jobsri, J.; Allen, A.; Rajagopal, D.; Shipton, M.; Kanyuka, K.; Lomonossoff, G.P.; Ottensmeier, C.; Diebold, S.S.; Stevenson, F.K.; Savelyeva, N. Plant virus particles carrying tumour antigen activate TLR7 and induce high levels of protective antibody. *PLoS ONE* **2015**, *10*, e0118096. [CrossRef] [PubMed]
118. Terhuja, M.; Saravanan, P.; Tamilselvan, R.P. Comparative efficacy of virus-like particle (VLP) vaccine of foot-and-mouth disease virus (FMDV) type O adjuvanted with poly I:C or CpG in guinea pigs. *Biologicals* **2015**, *43*, 437–443. [CrossRef] [PubMed]
119. Mohsen, M.O.; Gomes, A.C.; Vogel, M.; Bachmann, M.F. Interaction of viral capsid-derived virus-like particles (VLPs) with the innate immune system. *Vaccines* **2018**, *6*, 37. [CrossRef] [PubMed]
120. Yang, Z.; Chi, Y.; Bao, J.; Zhao, X.; Zhang, J.; Wang, L. Virus-like Particles for TEM Regulation and Antitumor Therapy. *J. Funct. Biomater.* **2022**, *13*, 304. [CrossRef]
121. Alexopoulou, L.; Holt, A.C.; Medzhitov, R.; Flavell, R.A. Recognition of double-stranded RNA and activation of NF-kappaB by Toll-like receptor 3. *Nature* **2001**, *413*, 732–738. [CrossRef]
122. Janeway, C.A., Jr.; Medzhitov, R. Innate immune recognition. *Annu. Rev. Immunol.* **2002**, *20*, 197–216. [CrossRef]
123. Akira, S.; Uematsu, S.; Takeuchi, O. Pathogen recognition and innate immunity. *Cell* **2006**, *124*, 783–801. [CrossRef] [PubMed]
124. Kawai, T.; Akira, S. The role of pattern-recognition receptors in innate immunity: Update on Toll-like receptors. *Nat. Immunol.* **2010**, *11*, 373–384. [CrossRef] [PubMed]
125. Gomes, A.C.; Roesti, E.S.; El-Turabi, A.; Bachmann, M.F. Type of RNA packed in VLPs impacts IgG class switching—Implications for an influenza vaccine design. *Vaccines* **2019**, *7*, 47. [CrossRef] [PubMed]
126. Krueger, C.C.; Thoms, F.; Keller, E.; Leoratti, F.M.S.; Vogel, M.; Bachmann, M.F. RNA and toll-like receptor 7 license the generation of superior secondary plasma cells at multiple levels in a B cell intrinsic fashion. *Front. Immunol.* **2019**, *10*, 736. [CrossRef] [PubMed]
127. Markine-Goriaynoff, D.; Coutelier, J.P. Increased efficacy of the immunoglobulin G2a subclass in antibody-mediated protection against lactate dehydrogenase-elevating virus-induced polioencephalomyelitis revealed with switch mutants. *J. Virol.* **2002**, *76*, 432–435. [CrossRef] [PubMed]
128. Weber, S.S.; Ducry, J.; Oxenius, A. Dissecting the contribution of IgG subclasses in restricting airway infection with Legionella pneumophila. *J. Immunol.* **2014**, *193*, 4053–4059. [CrossRef]
129. Novák, J.; Panská, L.; Macháček, T.; Kolářová, L.; Horák, P. Humoral response of mice infected with Toxocara canis following different infection schemes. *Acta Parasitol.* **2017**, *62*, 823–835. [CrossRef] [PubMed]
130. Hughes, H.R.; Crill, W.D.; Davis, B.S.; Chang, G.-J.J. A West Nile virus CD4 T cell epitope improves the immunogenicity of Dengue virus serotype 2 vaccines. *Virology* **2012**, *424*, 129–137. [CrossRef]
131. Del Guercio, M.F.; Alexander, J.; Kubo, R.T.; Arrhenius, T.; Maewal, A.; Appella, E.; Hoffman, S.L.; Jones, T.; Valmori, D.; Sakaguchi, K.; et al. Potent immunogenic short linear peptide constructs composed of B cell epitopes and pan DR T helper epitopes (PADRE) for antibody responses in vivo. *Vaccine* **1997**, *15*, 441–448. [CrossRef]
132. Ressing, M.E.; van Driel, W.J.; Brandt, R.M.; Kenter, G.G.; de Jong, J.H.; Bauknecht, T.; Fleuren, G.J.; Hoogerhout, P.; Offringa, R.; Sette, A.; et al. of T helper responses, but not of human papillomavirus-specific cytotoxic T lymphocyte responses, after peptide vaccination of patients with cervical carcinoma. *J. Immunother.* **2000**, *23*, 255–266. [CrossRef] [PubMed]
133. Chu, C.; Zhang, W.; Li, J.; Wan, Y.; Wang, Z.; Duan, R.; Yu, P.; Zhao, N.; Zhang, K.; Wang, S.; et al. A single codon optimization enhances recombinant human TNF-α vaccine expression in *Escherichia coli*. *BioMed. Res. Int.* **2018**, *2018*, 3025169. [CrossRef] [PubMed]
134. Micoli, F.; Adamo, R.; Costantino, P. Protein carriers for glycoconjugate vaccines: History, selection criteria, characterization and new trends. *Molecules* **2018**, *23*, 1451. [CrossRef] [PubMed]

135. Wu, Y.; Kelly, S.H.; Sanchez-Perez, L.; Sampson, J.H.; Collier, J.H. Comparative study of α-helical and β-sheet self-assembled peptide nanofiber vaccine platforms: Influence of integrated T-cell epitopes. *Biomater. Sci.* **2020**, *8*, 3522–3535. [CrossRef] [PubMed]

136. Panina-Bordignon, P.; Tan, A.; Termijtelen, A.; Demotz, S.; Corradin, G.; Lanzavecchia, A. Universally immunogenic T cell epitopes: Promiscuous binding to human MHC class II and promiscuous recognition by T cells. *Eur. J. Immunol.* **1989**, *19*, 2237–2242. [CrossRef] [PubMed]

137. Demotz, S.; Lanzavecchia, A.; Eisel, U.; Niemann, H.; Widmann, C.; Corradin, G. Delineation of several DR-restricted tetanus toxin T cell epitopes. *J. Immunol.* **1989**, *142*, 394–402. [CrossRef] [PubMed]

138. Chianese-Bullock, K.A.; Irvin, W.P., Jr.; Petroni, G.R.; Murphy, C.; Smolkin, M.; Olson, W.C.; Coleman, E.; Boerner, S.A.; Nail, C.J.; Neese, P.Y.; et al. A multipeptide vaccine is safe and elicits T-cell responses in participants with advanced stage ovarian cancer. *J. Immunother.* **2008**, *31*, 420–430. [CrossRef]

139. Rechtsteiner, G.; Warger, T.; Osterloh, P.; Schild, H.; Radsak, M.P. Cutting edge: Priming of CTL by transcutaneous peptide immunization with imiquimod. *J. Immunol.* **2005**, *174*, 2476–2480. [CrossRef] [PubMed]

140. Alexander, J.; Sidney, J.; Southwood, S.; Ruppert, J.; Oseroff, C.; Maewal, A.; Snoke, K.; Serra, H.M.; Kubo, R.T.; Sette, A.; et al. Development of high potency universal DR-restricted helper epitopes by modification of high affinity DR-blocking peptides. *Immunity* **1994**, *1*, 751–761. [CrossRef]

141. Alexander, J.; Fikes, J.; Hoffman, S.; Franke, E.; Sacci, J.; Appella, E.; Chisari, F.V.; Guidotti, L.G.; Chesnut, R.W.; Livingston, B.; et al. The optimization of helper T lymphocyte (HTL) function in vaccine development. *Immunol. Res.* **1998**, *18*, 79–92. [CrossRef]

142. Ochoa, R.; Lunardelli, V.A.S.; Rosa, D.S.; Laio, A.; Cossio, P. Multiple-Allele MHC Class II Epitope Engineering by a Molecular Dynamics-Based Evolution Protocol. *Front. Immunol.* **2022**, *13*, 862851. [CrossRef]

143. Wu, C.Y.; Monie, A.; Pang, X.; Hung, C.F.; Wu, T.C. Improving therapeutic HPV peptide-based vaccine potency by enhancing CD4+ T help and dendritic cell activation. *J. Biomed. Sci.* **2010**, *17*, 88. [CrossRef]

144. Li, S.; Peng, L.; Zhao, W.; Zhong, H.; Zhang, F.; Yan, Z.; Cao, H. Synthetic peptides containing B- and T-cell epitope of dengue virus-2 E domain III provoked B- and T-cell responses. *Vaccine* **2011**, *29*, 3695–3702. [CrossRef]

145. Wang, H.; Su, X.; Zhang, P.; Liang, J.; Wei, H.; Wan, M.; Wu, X.; Yu, Y.; Wang, L. Recombinant heat shock protein 65 carrying PADRE and HBV epitopes activates dendritic cells and elicits HBV-specific CTL responses. *Vaccine* **2011**, *29*, 2328–2335. [CrossRef]

146. La Rosa, C.; Longmate, J.; Lacey, S.F.; Kaltcheva, T.; Sharan, R.; Marsano, D.; Kwon, P.; Drake, J.; Williams, B.; Denison, S.; et al. Clinical evaluation of safety and immunogenicity of PADRE-cytomegalovirus (CMV) and tetanus-CMV fusion peptide vaccines with or without PF03512676 adjuvant. *J. Infect. Dis.* **2012**, *205*, 1294–1304. [CrossRef] [PubMed]

147. Feng, G.-d.; Xue, X.-c.; Gao, M.-l.; Wang, X.-f.; Shu, Z.; Mu, N.; Gao, Y.; Wang, Z.-l.; Hao, Q.; Li, W.-n.; et al. Therapeutic effects of PADRE-BAFF autovaccine on rat adjuvant arthritis. *BioMed. Res. Int.* **2014**, *2014*, 854954. [CrossRef] [PubMed]

148. El Bissati, K.; Chentoufi, A.A.; Krishack, P.A.; Zhou, Y.; Woods, S.; Dubey, J.P.; Vang, L.; Lykins, J.; Broderick, K.E.; Mui, E.; et al. Adjuvanted multi-epitope vaccines protect HLA-A*11, 01 transgenic mice against Toxoplasma gondii. *JCI Insight* **2016**, *1*, e85955. [CrossRef] [PubMed]

149. Snook, A.E.; Baybutt, T.R.; Hyslop, T.; Waldman, S.A. Preclinical evaluation of a replication-deficient recombinant adenovirus serotype 5 vaccine expressing guanylate cyclase C and the PADRE T-helper epitope. *Hum. Gene Ther. Methods* **2016**, *27*, 238–250. [CrossRef]

150. El Bissati, K.; Zhou, Y.; Paulillo, S.M.; Raman, S.K.; Karch, C.P.; Roberts, C.W.; Lanar, D.E.; Reed, S.; Fox, C.; Carter, D.; et al. Protein nanovaccine confers robust immunity against toxoplasma. *NPJ Vaccines* **2017**, *2*, 24. [CrossRef]

151. Safavi, A.; Kefayat, A.; Mahdevar, E.; Abiri, A.; Ghahremani, F. Exploring the out of sight antigens of SARS-CoV-2 to design a candidate multi-epitope vaccine by utilizing immunoinformatics approaches. *Vaccine* **2020**, *38*, 7612–7628. [CrossRef]

152. Alexander, J.; del Guercio, M.F.; Maewal, A.; Qiao, L.; Fikes, J.; Chesnut, R.W.; Paulson, J.; Bundle, D.R.; DeFrees, S.; Sette, A. Linear PADRE T helper epitope and carbohydrate B cell epitope conjugates induce specific high titer IgG antibody responses. *J. Immunol.* **2000**, *164*, 1625–1633. [CrossRef] [PubMed]

153. Alexander, J.; del Guercio, M.F.; Frame, B.; Maewal, A.; Sette, A.; Nahm, M.H.; Newman, M.J. Development of experimental carbohydrate-conjugate vaccines composed of Streptococcus pneumoniae capsular polysaccharides and the universal helper T-lymphocyte epitope (PADRE). *Vaccine* **2004**, *22*, 2362–2367. [CrossRef] [PubMed]

154. Hung, C.F.; Tsai, Y.C.; He, L.; Wu, T.C. DNA vaccines encoding Ii-PADRE generates potent PADRE-specific CD4+ T-cell immune responses and enhances vaccine potency. *Mol. Ther.* **2007**, *15*, 1211–1219. [CrossRef] [PubMed]

155. Ghaffari-Nazari, H.; Tavakkol-Afshari, J.; Jaafari, M.R.; Tahaghoghi-Hajghorbani, S.; Masoumi, E.; Jalali, S.A. Improving multi-epitope long peptide vaccine potency by using a strategy that enhances CD4+ T help in BALB/c mice. *PLoS ONE* **2015**, *10*, e0142563. [CrossRef] [PubMed]

156. Zamani, P.; Teymouri, M.; Nikpoor, A.R.; Gholizadeh Navashenaq, J.; Gholizadeh, Z.; Amiri Darban, S.; Jaafari, M.R. Nanoliposomal vaccine containing long multi-epitope peptide E75-AE36 pulsed PADRE-induced effective immune response in mice TuBo model of breast cancer. *Eur. J. Cancer* **2020**, *129*, 80–96. [CrossRef]

157. Pompano, R.R.; Chen, J.; Verbus, E.A.; Han, H.; Fridman, A.; McNeely, T.; Collier, J.H.; Chong, A.S. Titrating T-cell epitopes within self-assembled vaccines optimizes CD4+ helper T cell and antibody outputs. *Adv. Health Mater.* **2014**, *3*, 1898–1908. [CrossRef] [PubMed]

158. Wu, Y.; Norberg, P.K.; Reap, E.A.; Congdon, K.L.; Fries, C.N.; Kelly, S.H.; Sampson, J.H.; Conticello, V.P.; Collier, J.H. A Supramolecular Vaccine Platform Based on α-Helical Peptide Nanofibers. *ACS Biomater. Sci. Eng.* **2017**, *3*, 3128–3132. [CrossRef] [PubMed]

159. Shores, L.S.; Kelly, S.H.; Hainline, K.M.; Suwanpradid, J.; MacLeod, A.S.; Collier, J.H. Multifactorial design of a supramolecular peptide anti-IL-17 vaccine toward the treatment of psoriasis. *Front. Immunol.* **2020**, *11*, 1855. [CrossRef] [PubMed]

160. Krenger, P.S.; Josi, R.; Sobczak, J.; Velazquez, T.L.C.; Balke, I.; Skinner, M.A.; Kramer, M.F.; Scott, C.J.W.; Hewings, S.; Heath, M.D. Influence of antigen density and TLR ligands on preclinical efficacy of a VLP-based vaccine against peanut allergy. *Allergy* **2024**, *79*, 184–199. [CrossRef]

161. Kozlovska, T.M.; Cielens, I.; Dreilina, D.; Dislers, A.; Baumanis, V.; Ose, V.; Pumpens, P. Recombinant RNA phage Q beta capsid particles synthesized and self-assembled in *Escherichia coli*. *Gene* **1993**, *137*, 133–137. [CrossRef]

162. Fettelschoss-Gabriel, A.; Fettelschoss, V.; Olomski, F.; Birkmann, K.; Thoms, F.; Buhler, M.; Kummer, M.; Zeltins, A.; Kundig, T.M.; Bachmann, M.F. Active vaccination against interleukin-5 as long-term treatment for insect-bite hypersensitivity in horses. *Allergy* **2019**, *74*, 572–582. [CrossRef] [PubMed]

163. Chang, X.; Liu, X.; Mohsen, M.O.; Zeltins, A.; Martina, B.; Vogel, M.; Bachmann, M.F. Induction of Broadly Cross-Reactive Antibodies by Displaying Receptor Binding Domains of SARS-CoV-2 on Virus-like Particles. *Vaccines* **2022**, *10*, 307. [CrossRef]

164. Rothen, D.A.; Krenger, P.S.; Nonic, A.; Balke, I.; Vogt, A.C.S.; Chang, X.; Manenti, A.; Vedovi, F.; Resevica, G.; Walton, S.M.; et al. Intranasal administration of a virus-like particles-based vaccine induces neutralizing antibodies against SARS-CoV-2 and variants of concern. *Allergy* **2022**, *77*, 2446–2458. [CrossRef]

165. Varanda, C.M.R.; Machado, M.; Martel, P.; Nolasco, G.; Clara, M.I.E.; Félix, M.R. Genetic diversity of the coat protein of olive mild mosaic virus (OMMV) and tobacco necrosis virus D (TNV-D) isolates and its structural implications. *PLoS ONE* **2014**, *9*, e110941. [CrossRef]

166. Smith, T.J.; Chase, E.; Schmidt, T.; Perry, K.L. The structure of cucumber mosaic virus and comparison to cowpea chlorotic mottle virus. *J. Virol.* **2000**, *74*, 7578–7586. [CrossRef]

167. Percival-Alwyn, J.L.; England, E.; Kemp, B.; Rapley, L.; Davis, N.H.E.; McCarthy, G.R.; Majithiya, J.B.; Corkill, D.J.; Welsted, S.; Minton, K.; et al. Generation of potent mouse monoclonal antibodies to self-proteins using T-cell epitope "tags". *MAbs* **2015**, *7*, 129–137. [CrossRef] [PubMed]

168. Skelton, D.; Satake, N.; Kohn, D.B. The enhanced green fluorescent protein (eGFP) is minimally immunogenic in C57BL/6 mice. *Gene Ther.* **2001**, *8*, 1813–1814. [CrossRef] [PubMed]

169. Chen, D.J.; Osterrieder, N.; Metzger, S.M.; Buckles, E.; Doody, A.M.; DeLisa, M.P.; Putnam, D. Delivery of foreign antigens by engineered outer membrane vesicle vaccines. *Proc. Natl. Acad. Sci. USA* **2010**, *107*, 3099–3104. [CrossRef]

170. Mairuhu, A.T.; Wagenaar, J.; Brandjes, D.P.; van Gorp, E.C. Dengue: An arthropod-borne disease of global importance. *Eur. J. Clin. Microbiol. Infect. Dis.* **2004**, *23*, 425–433. [CrossRef]

171. Guzman, M.G.; Halstead, S.B.; Artsob, H.; Buchy, P.; Farrar, J.; Gubler, D.J.; Hunsperger, E.; Kroeger, A.; Margolis, H.S.; Martínez, E.; et al. Dengue: A continuing global threat. *Nat. Rev. Microbiol.* **2010**, *8* (Suppl. S12), S7–S16. [CrossRef]

172. Khetarpal, N.; Khanna, I. Dengue fever: Causes, complications, and vaccine strategies. *J. Immunol. Res.* **2016**, *2016*, 6803098. [CrossRef] [PubMed]

173. Guzman, M.G.; Hermida, L.; Bernardo, L.; Ramirez, R.; Guillén, G. Domain III of the envelope protein as a dengue vaccine target. *Expert Rev. Vaccines* **2010**, *9*, 137–147. [CrossRef] [PubMed]

174. Fahimi, H.; Mohammadipour, M.; Haddad Kashani, H.; Parvini, F.; Sadeghizadeh, M. Dengue viruses and promising envelope protein domain III-based vaccines. *Appl. Microbiol. Biotechnol.* **2018**, *102*, 2977–2996. [CrossRef] [PubMed]

175. Seesen, M.; Jearanaiwitayakul, T.; Limthongkul, J.; Midoeng, P.; Sunintaboon, P.; Ubol, S. A bivalent form of nanoparticle-based dengue vaccine stimulated responses that potently eliminate both DENV-2 particles and DENV-2-infected cells. *Vaccine* **2023**, *41*, 1638–1648. [CrossRef]

176. Gromowski, G.D.; Barrett, A.D. Characterization of an antigenic site that contains a dominant, type-specific neutralization determinant on the envelope protein domain III (ED3) of dengue 2 virus. *Virology* **2007**, *366*, 349–360. [CrossRef] [PubMed]

177. Sukupolvi-Petty, S.; Austin, S.K.; Purtha, W.E.; Oliphant, T.; Nybakken, G.E.; Schlesinger, J.J.; Roehrig, J.T.; Gromowski, G.D.; Barrett, A.D.; Fremont, D.H.; et al. Type- and subcomplex-specific neutralizing antibodies against domain III of dengue virus type 2 envelope protein recognize adjacent epitopes. *J. Virol.* **2007**, *81*, 12816–12826. [CrossRef]

178. Gromowski, G.D.; Barrett, N.D.; Barrett, A.D.T. Characterization of dengue virus complex-specific neutralizing epitopes on envelope protein domain III of dengue 2 virus. *J. Virol.* **2008**, *82*, 8828–8837. [CrossRef]

179. Chen, H.W.; Liu, S.J.; Li, Y.S.; Liu, H.H.; Tsai, J.P.; Chiang, C.Y.; Chen, M.Y.; Hwang, C.S.; Huang, C.C.; Hu, H.M.; et al. A consensus envelope protein domain III can induce neutralizing antibody responses against serotype 2 of dengue virus in non-human primates. *Arch. Virol.* **2013**, *158*, 1523–1531. [CrossRef]

180. Rajpoot, R.K.; Shukla, R.; Arora, U.; Swaminathan, S.; Khanna, N. Dengue envelope-based 'four-in-one' virus-like particles produced using Pichia pastoris induce enhancement-lacking, domain III-directed tetravalent neutralising antibodies in mice. *Sci. Rep.* **2018**, *8*, 8643. [CrossRef]

181. Shukla, R.; Rajpoot, R.K.; Arora, U.; Poddar, A.; Swaminathan, S.; Khanna, N. Pichia pastoris-Expressed Bivalent Virus-Like Particulate Vaccine Induces Domain III-Focused Bivalent Neutralizing Antibodies without Antibody-Dependent Enhancement in Vivo. *Front. Microbiol.* **2018**, *8*, 2644. [CrossRef]

182. Ramasamy, V.; Arora, U.; Shukla, R.; Poddar, A.; Shanmugam, R.K.; White, L.J.; Mattocks, M.M.; Raut, R.; Perween, A.; Tyagi, P.; et al. A tetravalent virus-like particle vaccine designed to display domain III of dengue envelope proteins induces multi-serotype neutralizing antibodies in mice and macaques which confer protection against antibody dependent enhancement in AG129 mice. *PLoS Negl. Trop. Dis.* **2018**, *12*, e0006191. [CrossRef]
183. Huang, H.-J.; Yang, M.; Chen, H.-W.; Wang, S.; Chang, C.-P.; Ho, T.-S.; Kao, Y.-S.; Tien, S.-M.; Lin, H.-H.; Chang, P.-C.; et al. A novel chimeric dengue vaccine candidate composed of consensus envelope protein domain III fused to C-terminal-modified NS1 protein. *Vaccine* **2022**, *40*, 2299–2310. [CrossRef]
184. Spohn, G.; Jennings, G.T.; Martina, B.E.; Keller, I.; Beck, M.; Pumpens, P.; Osterhaus, A.D.M.E.; Bachmann, M.F. A VLP-based vaccine targeting domain III of the West Nile virus E protein protects from lethal infection in mice. *Virol. J.* **2010**, *7*, 146. [CrossRef]
185. Maeda, Y.; Ueda, H.; Kazami, J.; Kawano, G.; Suzuki, E.; Nagamune, T. Engineering of functional chimeric protein G–Vargula luciferase. *Anal. Biochem.* **1997**, *249*, 147–152. [CrossRef]
186. Kalnciema, I.; Balke, I.; Skrastina, D.; Ose, V.; Zeltins, A. Potato virus M-like nanoparticles: Construction and characterization. *Mol. Biotechnol.* **2015**, *57*, 982–992. [CrossRef]
187. Qi, X.; Sun, Y.; Xiong, S. A single freeze-thawing cycle for highly efficient solubilization of inclusion body proteins and its refolding into bioactive form. *Microb. Cell Fact.* **2015**, *14*, 24. [CrossRef] [PubMed]
188. Linke, T.; Aspelund, M.T.; Thompson, C.; Xi, G.; Fulton, A.; Wendeler, M.; Pabst, T.M.; Wang, X.; Wang, W.K.; Ram, K.; et al. Development and scale-up of a commercial fed batch refolding process for an anti-CD22 two chain immunotoxin. *Biotechnol. Prog.* **2014**, *30*, 1380–1389. [CrossRef] [PubMed]
189. Fink, A.L. Protein aggregation: Folding aggregates, inclusion bodies and amyloid. *Fold Des.* **1998**, *3*, R9–R23. [CrossRef] [PubMed]
190. Geier, M.R.; Stanbro, H.; Merril, C.R. Endotoxins in commercial vaccines. *Appl. Environ. Microbiol.* **1978**, *36*, 445–449. [CrossRef]
191. Malyala, P.; Singh, M. Endotoxin limits in formulations for preclinical research. *J. Pharm. Sci.* **2008**, *97*, 2041–2044. [CrossRef]
192. Brito, L.A.; Singh, M. Acceptable levels of endotoxin in vaccine formulations during preclinical research. *J. Pharm. Sci.* **2011**, *100*, 34–37. [CrossRef] [PubMed]
193. Rio, D.C.; Ares, M., Jr.; Hannon, G.J.; Nilsen, T.W. Purification of RNA using TRIzol (TRI reagent). *Cold Spring Harb. Protoc.* **2010**, *2010*, pdb.prot5439. [CrossRef]
194. Nair, S.; Savithri, H.S. Natively unfolded nucleic acid binding P8 domain of SeMV polyprotein 2a affects the novel ATPase activity of the preceding P10 domain. *FEBS Lett.* **2010**, *584*, 571–576. [CrossRef] [PubMed]
195. Hønsvall, B.K.; Robertson, L.J. Washed Away; How Not to Lose Your RNA during Isolation. *J. Biomol. Tech.* **2017**, *28*, 75–79. [CrossRef]
196. Braun, M.; Jandus, C.; Maurer, P.; Hammann-Haenni, A.; Schwarz, K.; Bachmann, M.F.; Speiser, D.E.; Romero, P. Virus-like particles induce robust human T-helper cell responses. *Eur. J. Immunol.* **2012**, *42*, 330–340. [CrossRef]
197. Farlow, M.R.; Andreasen, N.; Riviere, M.E.; Vostiar, I.; Vitaliti, A.; Sovago, J.; Caputo, A.; Winblad, B.; Graf, A. Long-term treatment with active Aβ immunotherapy with CAD106 in mild Alzheimer's disease. *Alzheimers Res. Ther.* **2015**, *7*, 23. [CrossRef] [PubMed]
198. Vandenberghe, R.; Riviere, M.E.; Caputo, A.; Sovago, J.; Maguire, R.P.; Farlow, M.; Marotta, G.; Sanchez-Valle, R.; Scheltens, P.; Ryan, J.M.; et al. Active Aβ immunotherapy CAD106 in Alzheimer's disease: A phase 2b study. *Alzheimers Dement.* **2017**, *3*, 10–22. [CrossRef]
199. Classen, D.C.; Morningstar, J.M.; Shanley, J.D. Detection of antibody to murine cytomegalovirus by enzyme-linked immunosorbent and indirect immunofluorescence assays. *J. Clin. Microbiol.* **1987**, *25*, 600–604. [CrossRef] [PubMed]
200. Lardeux, F.; Torrico, G.; Aliaga, C. Calculation of the ELISA's cut-off based on the change-point analysis method for detection of Trypanosoma cruzi infection in Bolivian dogs in the absence of controls. *Mem. Inst. Oswaldo Cruz.* **2016**, *111*, 501–504. [CrossRef]
201. Fick de Souza, V.A.U.; Fernandes, S.; Araújo, E.S.; Tateno, A.F.; Oliveira, O.M.N.P.F.; Oliveira, R.d.R.; Pannuti, C.S. Use of an Immunoglobulin G Avidity Test to Discriminate between Primary and Secondary Dengue Virus Infections. *J. Clin. Microbiol.* **2004**, *42*, 1782–1784. [CrossRef]
202. Olsson, J.; Johansson, J.; Honkala, E.; Blomqvist, B.; Kok, E.; Weidung, B.; Lövheim, H.; Elgh, F. Urea dilution of serum for reproducible anti-HSV1 IgG avidity index. *BMC Infect. Dis.* **2019**, *19*, 164. [CrossRef] [PubMed]
203. Correa, V.A.; Rodrigues, T.S.; Portilho, A.I.; Lima, G.T.; De Gaspari, E. Modified ELISA for antibody avidity evaluation: The need for standardization. *Biomed. J.* **2021**, *44*, 433–438. [CrossRef] [PubMed]
204. Nurmi, V.; Hedman, L.; Perdomo, M.F.; Weseslindtner, L.; Hedman, K. Comparison of approaches for IgG avidity calculation and a new highly sensitive and specific method with broad dynamic range. *Int. J. Infect. Dis.* **2021**, *110*, 479–487. [CrossRef] [PubMed]
205. Balke, I.; Silamikelis, I.; Radovica-Spalvina, I.; Zeltina, V.; Resevica, G.; Fridmanis, D.; Zeltins, A. Ryegrass mottle virus complete genome determination and development of infectious cDNA by combining two methods-3' RACE and RNA-Seq. *PLoS ONE* **2023**, *18*, e0287278. [CrossRef] [PubMed]
206. Ribas, A.; Medina, T.; Kirkwood, J.M.; Zakharia, Y.; Gonzalez, R.; Davar, D.; Chmielowski, B.; Campbell, K.M.; Bao, R.; Kelley, H.; et al. Overcoming PD-1 Blockade Resistance with CpG-A Toll-Like Receptor 9 Agonist Vidutolimod in Patients with Metastatic Melanoma. *Cancer Discov.* **2021**, *11*, 2998–3007. [CrossRef] [PubMed]
207. Mellid-Carballal, R.; Gutierrez-Gutierrez, S.; Rivas, C.; Garcia-Fuentes, M. Viral protein-based nanoparticles (part 2): Pharmaceutical applications. *Eur. J. Pharm. Sci.* **2023**, *189*, 106558. [CrossRef] [PubMed]
208. Matsuura, K. Construction of spherical virus-inspired peptide nanoassemblies. *Polym. J.* **2012**, *44*, 469–474. [CrossRef]

209. Janković, P.; Šantek, I.; Pina, A.S.; Kalafatovic, D. Exploiting peptide self-assembly for the development of minimalistic viral mimetics. *Front. Chem.* **2021**, *9*, 723473. [CrossRef]

210. Rötzschke, O.; Falk, K.; Strominger, J.L. Superactivation of an immune response triggered by oligomerized T cell epitopes. *Proc. Natl. Acad. Sci. USA* **1997**, *94*, 14642–14647. [CrossRef]

211. Fossum, E.; Grødeland, G.; Terhorst, D.; Tveita, A.A.; Vikse, E.; Mjaaland, S.; Henri, S.; Malissen, B.; Bogen, B. Vaccine molecules targeting XCR1 on cross-presenting DCs induce protective CD8+ T-cell responses against influenza virus. *Eur. J. Immunol.* **2015**, *45*, 624–635. [CrossRef]

212. Grødeland, G.; Fossum, E.; Bogen, B. Polarizing T and B cell responses by APC-targeted subunit vaccines. *Front. Immunol.* **2015**, *6*, 367. [CrossRef] [PubMed]

213. Bournazos, S.; Klein, F.; Pietzsch, J.; Seaman, M.S.; Nussenzweig, M.C.; Ravetch, J.V. Broadly neutralizing anti-HIV-1 antibodies require Fc effector functions for in vivo activity. *Cell* **2014**, *158*, 1243–1253. [CrossRef] [PubMed]

214. DiLillo, D.J.; Tan, G.S.; Palese, P.; Ravetch, J.V. Broadly neutralizing hemagglutinin stalk-specific antibodies require FcγR interactions for protection against influenza virus in vivo. *Nat. Med.* **2014**, *20*, 143–151. [CrossRef] [PubMed]

215. Visciano, M.L.; Tagliamonte, M.; Tornesello, M.L.; Buonaguro, F.M.; Buonaguro, L. Effects of adjuvants on IgG subclasses elicited by virus-like particles. *J. Transl. Med.* **2012**, *10*, 4. [CrossRef]

216. Samal, S.; Shrivastava, T.; Sonkusre, P.; Rizvi, Z.A.; Kumar, R.; Ahmed, S.; Vishwakarma, P.; Yadav, N.; Bansal, M.; Chauhan, K.; et al. Tetramerizing TGCN4 domain facilitates production of influenza A H1N1 M2e higher order soluble oligomers that show enhanced immunogenicity in vivo. *J. Biol. Chem.* **2020**, *295*, 14352–14366. [CrossRef] [PubMed]

217. Wang, S.; Heilman, D.; Liu, F.; Giehl, T.; Joshi, S.; Huang, X.; Chou, T.; Goguen, J.; Lu, S. A DNA vaccine producing LcrV antigen in oligomers is effective in protecting mice from lethal mucosal challenge of plague. *Vaccine* **2004**, *22*, 3348–3357. [CrossRef] [PubMed]

218. Dalgediene, I.; Lasickiene, R.; Budvytyte, R.; Valincius, G.; Morkuniene, R.; Borutaite, V.; Zvirbliene, A. Immunogenic properties of amyloid beta oligomers. *J. Biomed. Sci.* **2013**, *20*, 10. [CrossRef]

219. Perlmutter, R.M.; Hansburg, D.; Briles, D.E.; Nicolotti, R.A.; Davie, J.M. Subclass restriction of murine anti-carbohydrate antibodies. *J. Immunol.* **1978**, *121*, 566–572. [CrossRef]

220. Slack, J.; Der-Balian, G.P.; Nahm, M.; Davie, J.M. Subclass restriction of murine antibodies. II. The IgG plaque-forming cell response to thymus-independent type 1 and type 2 antigens in normal mice and mice expressing an X-linked immunodeficiency. *J. Exp. Med.* **1980**, *151*, 853–862. [CrossRef]

221. Coutelier, J.P.; van der Logt, J.T.; Heessen, F.W.; Warnier, G.; Van Snick, J. IgG2a restriction of murine antibodies elicited by viral infections. *J. Exp. Med.* **1987**, *165*, 64–69. [CrossRef]

222. Coutelier, J.P.; van der Logt, J.T.; Heessen, F.W. IgG subclass distribution of primary and secondary immune responses concomitant with viral infection. *J. Immunol.* **1991**, *147*, 1383–1386. [CrossRef] [PubMed]

223. Modis, Y.; Ogata, S.; Clements, D.; Harrison, S.C. Structure of the dengue virus envelope protein after membrane fusion. *Nature* **2004**, *427*, 313–319. [CrossRef] [PubMed]

224. Kuhn, R.J.; Zhang, W.; Rossmann, M.G.; Pletnev, S.V.; Corver, J.; Lenches, E.; Jones, C.T.; Mukhopadhyay, S.; Chipman, P.R.; Strauss, E.G.; et al. Structure of dengue virus: Implications for flavivirus organization, maturation, and fusion. *Cell* **2002**, *108*, 717–725. [CrossRef]

225. Matsuura, K.; Shiomi, Y.; Mizuta, T.; Inaba, H. Horseradish peroxidase-decorated artificial viral capsid constructed from beta-annulus peptide via interaction between his-tag and ni-nta. *Processes* **2020**, *8*, 1455. [CrossRef]

226. Chacón-Díaz, C.; Muñoz-Rodríguez, M.; Barquero-Calvo, E.; Guzmán-Verri, C.; Chaves-Olarte, E.; Grilló, M.J.; Moreno, E. The use of green fluorescent protein as a marker for brucella vaccines. *Vaccine* **2011**, *29*, 577–582. [CrossRef] [PubMed]

227. Bachmann, M.F.; Zinkernagel, R.M. The influence of virus structure on antibody responses and virus serotype formation. *Immunol. Today* **1996**, *17*, 553–558. [CrossRef]

228. Poteet, E.; Lewis, P.; Chen, C.; Ho, S.O.; Do, T.; Chiang, S.; Labranche, C.; Montefiori, D.; Fujii, G.; Yao, Q. Toll-like receptor 3 adjuvant in combination with virus-like particles elicit a humoral response against HIV. *Vaccine* **2016**, *34*, 5886–5894. [CrossRef]

229. Gomes, A.C.; Mohsen, M.O.; Mueller, J.E.; Leoratti, F.M.S.; Cabral-Miranda, G.; Bachmann, M.F. Early transcriptional signature in dendritic cells and the induction of protective T cell responses upon immunization with VLPs containing TLR ligands-a role for CCL2. *Front. Immunol.* **2019**, *10*, 1679. [CrossRef] [PubMed]

230. Kasturi, S.P.; Kozlowski, P.A.; Nakaya, H.I.; Burger, M.C.; Russo, P.; Pham, M.; Kovalenkov, Y.; Silveira, E.L.V.; Havenar-Daughton, C.; Burton, S.L.; et al. Adjuvanting a simian immunodeficiency virus vaccine with toll-like receptor ligands encapsulated in nanoparticles induces persistent antibody responses and enhanced protection in TRIM5α restrictive macaques. *J. Virol.* **2017**, *91*, e01844-16. [CrossRef]

231. Mitragotri, S.; Anderson, D.G.; Chen, X.; Chow, E.K.; Ho, D.; Kabanov, A.V.; Karp, J.M.; Kataoka, K.; Mirkin, C.A.; Petrosko, S.H.; et al. Accelerating the translation of nanomaterials in biomedicine. *ACS Nano* **2015**, *9*, 6644–6654. [CrossRef]

232. Hoshyar, N.; Gray, S.; Han, H.; Bao, G. The effect of nanoparticle size on in vivo pharmacokinetics and cellular interaction. *Nanomedicine* **2016**, *11*, 673–692. [CrossRef] [PubMed]

233. Hirota, K.; Hasegawa, T.; Hinata, H.; Ito, F.; Inagawa, H.; Kochi, C.; Soma, G.-I.; Makino, K.; Terada, H. Optimum conditions for efficient phagocytosis of rifampicin-loaded PLGA microspheres by alveolar macrophages. *J. Control. Release* **2007**, *119*, 69–76. [CrossRef] [PubMed]

234. Lico, C.; Santi, L.; Twyman, R.M.; Pezzotti, M.; Avesani, L. The use of plants for the production of therapeutic human peptides. *Plant Cell Rep.* **2012**, *31*, 439–451. [PubMed]

235. Plotkin, S.A. Immunologic correlates of protection induced by vaccination. *Pediatr. Infect. Dis. J.* **2001**, *20*, 63–75. [CrossRef] [PubMed]

236. Plotkin, S.A. Vaccines: Correlates of vaccine-induced immunity. *Clin. Infect. Dis.* **2008**, *47*, 401–409. [CrossRef] [PubMed]

237. Plotkin, S.A. Correlates of protection induced by vaccination. *Clin. Vaccine Immunol.* **2010**, *17*, 1055–1065. [CrossRef] [PubMed]

238. Singh, G.; Abbad, A.; Tcheou, J.; Mendu, D.R.; Firpo-Betancourt, A.; Gleason, C.; Srivastava, K.; Cordon-Cardo, C.; Simon, V.; Krammer, F.; et al. Binding and Avidity Signatures of Polyclonal Sera from Individuals with Different Exposure Histories to Severe Acute Respiratory Syndrome Coronavirus 2 Infection, Vaccination, and Omicron Breakthrough Infections. *J. Infect. Dis.* **2023**, *228*, 564–575. [CrossRef] [PubMed]

239. Wu, J.; Mu, H.; Pan, X.; Guo, W. Studying the effects of booster shots and antibody responses to the SARS-CoV-2 vaccination over time in health personnel. *Front. Cell. Infect. Microbiol.* **2023**, *13*, 1138631. [CrossRef] [PubMed]

240. Puschnik, A.; Lau, L.; Cromwell, E.A.; Balmaseda, A.; Zompi, S.; Harris, E. Correlation between dengue-specific neutralizing antibodies and serum avidity in primary and secondary dengue virus 3 natural infections in humans. *PLoS Negl. Trop. Dis.* **2013**, *7*, e2274. [CrossRef]

241. Saron, W.A.A.; Rathore, A.P.S.; Ting, L.; Ooi, E.E.; Low, J.; Abraham, S.N.; St John, A.L. Flavivirus serocomplex cross-reactive immunity is protective by activating heterologous memory CD4 T cells. *Sci. Adv.* **2018**, *4*, eaar4297. [CrossRef]

242. Zepeda-Cervantes, J.; Ramírez-Jarquín, J.O.; Vaca, L. Interaction between Virus-like Particles (VLPs) and Pattern Recognition Receptors (PRRs) From Dendritic Cells (DCs): Toward Better Engineering of VLPs. *Front. Immunol.* **2020**, *11*, 1100. [CrossRef] [PubMed]

243. Armero-Gimenez, J.; Wilbers, R.; Schots, A.; Williams, C.; Finnern, R. Rapid screening and scaled manufacture of immunogenic virus-like particles in a tobacco BY-2 cell-free protein synthesis system. *Front. Immunol.* **2023**, *14*, 1088852. [CrossRef] [PubMed]

244. Zupančič, E.; Curato, C.; Paisana, M.; Rodrigues, C.; Porat, Z.; Viana, A.S.; Afonso, C.A.M.; Pinto, J.; Gaspar, R.; Moreira, J.N.; et al. Rational design of nanoparticles towards targeting antigen-presenting cells and improved T cell priming. *J. Control. Release* **2017**, *258*, 182–195. [CrossRef] [PubMed]

245. Shang, W.; Liu, J.; Yang, J.; Hu, Z.; Rao, X. Dengue virus-like particles: Construction and application. *Appl. Microbiol. Biotechnol.* **2012**, *94*, 39–46. [CrossRef] [PubMed]

246. Zhang, N.; Li, C.; Jiang, S.; Du, L. Recent Advances in the Development of Virus-Like Particle-Based Flavivirus Vaccines. *Vaccines* **2020**, *8*, 481. [CrossRef] [PubMed]

247. Castilho, L.R.; Mattos, N.R.; Abreu, W.S.; Gutarra, M.L.E. Virus-like Particles (VLPs) as Important Tools for Flavivirus Vaccine Development. *Biologics* **2022**, *2*, 226–242. [CrossRef]

248. Khetarpal, N.; Poddar, A.; Nemani, S.K.; Dhar, N.; Patil, A.; Negi, P.; Perween, A.; Viswanathan, R.; Lünsdorf, H.; Tyagi, P.; et al. Dengue-specific subviral nanoparticles: Design, creation and characterization. *J. Nanobiotechnol.* **2013**, *11*, 15–241. [CrossRef] [PubMed]

249. Venkataraman, S.; Hefferon, K. Application of plant viruses in biotechnology, medicine, and human health. *Viruses* **2021**, *13*, 1697. [CrossRef] [PubMed]

250. Peabody, D.S.; Peabody, J.; Bradfute, S.B.; Chackerian, B. RNA phage VLP-based vaccine platforms. *Pharmaceuticals* **2021**, *14*, 764. [CrossRef]

251. Warner, N.L.; Frietze, K.M. Development of Bacteriophage Virus-Like Particle Vaccines Displaying Conserved Epitopes of Dengue Virus Non-Structural Protein 1. *Vaccines* **2021**, *9*, 726. [CrossRef]

252. Didierlaurent, A.M.; Morel, S.; Lockman, L.; Giannini, S.L.; Bisteau, M.; Carlsen, H.; Kielland, A.; Vosters, O.; Vanderheyde, N.; Schiavetti, F.; et al. AS04, an aluminum salt- and TLR4 agonist-based adjuvant system, induces a transient localized innate immune response leading to enhanced adaptive immunity. *J. Immunol.* **2009**, *183*, 6186–6197. [CrossRef] [PubMed]

253. Ko, K.H.; Cha, S.B.; Lee, S.-H.; Bae, H.S.; Ham, C.S.; Lee, M.-G.; Kim, D.-H.; Han, S.H. A novel defined TLR3 agonist as an effective vaccine adjuvant. *Front. Immunol.* **2023**, *14*, 1075291. [CrossRef] [PubMed]

254. Bessa, J.; Jegerlehner, A.; Hinton, H.J.; Pumpens, P.; Saudan, P.; Schneider, P.; Bachmann, M.F. Alveolar macrophages and lung dendritic cells sense RNA and drive mucosal IgA responses. *J. Immunol.* **2009**, *183*, 3788–3799. [CrossRef] [PubMed]

255. Chang, X.; Krenger, P.; Krueger, C.C.; Zha, L.; Han, J.; Yermanos, A.; Roongta, S.; Mohsen, M.O.; Oxenius, A.; Vogel, M.; et al. TLR7 Signaling Shapes and Maintains Antibody Diversity upon Virus-like Particle Immunization. *Front. Immunol.* **2022**, *12*, 827256. [CrossRef] [PubMed]

256. Clausi, A.; Cummiskey, J.; Merkley, S.; Carpenter, J.F.; Jones Braun, L.; Randolph, T.W. Influence of particle size and antigen binding on effectiveness of aluminum salt adjuvants in a model lysozyme vaccine. *J. Pharm. Sci.* **2008**, *97*, 5252–5262. [CrossRef] [PubMed]

257. Coria, L.M.; Saposnik, L.M.; Castro, C.P.; Castro, E.F.; Bruno, L.A.; Stone, W.B.; Pérez, P.S.; Darriba, M.L.; Chemes, L.B.; Alcain, J.; et al. A Novel Bacterial Protease Inhibitor Adjuvant in RBD-Based COVID-19 Vaccine Formulations Containing Alum Increases Neutralizing Antibodies, Specific Germinal Center B Cells and Confers Protection against SARS-CoV-2 Infection in Mice. *Front. Immunol.* **2022**, *13*, 844837. [CrossRef] [PubMed]

258. Pardi, N.; Hogan, M.J.; Porter, F.W.; Weissman, D. mRNA vaccines—A new era in vaccinology. *Nat. Rev. Drug Discov.* **2018**, *17*, 261–279. [CrossRef] [PubMed]

259. Verbeke, R.; Hogan, M.J.; Loré, K.; Pardi, N. Innate immune mechanisms of mRNA vaccines. *Immunity* **2022**, *55*, 1993–2005. [CrossRef] [PubMed]

260. Muslimov, A.; Tereshchenko, V.; Shevyrev, D.; Rogova, A.; Lepik, K.; Reshetnikov, V.; Ivanov, R. The Dual Role of the Innate Immune System in the Effectiveness of mRNA Therapeutics. *Int. J. Mol. Sci.* **2023**, *24*, 14820. [CrossRef]

261. Diebold, S.S.; Massacrier, C.; Akira, S.; Paturel, C.; Morel, Y.; Reis e Sousa, C. Nucleic acid agonists for toll-like receptor 7 are defined by the presence of uridine ribonucleotides. *Eur. J. Immunol.* **2006**, *36*, 3256–3267. [CrossRef]

262. Zhang, Z.; Ohto, U.; Shimizu, T. Toward a structural understanding of nucleic acid-sensing toll-like receptors in the innate immune system. *FEBS Lett.* **2017**, *591*, 3167–3181. [CrossRef]

263. Sakaniwa, K.; Fujimura, A.; Shibata, T.; Shigematsu, H.; Ekimoto, T.; Yamamoto, M.; Ikeguchi, M.; Miyake, K.; Ohto, U.; Shimizu, T. TLR3 forms a laterally aligned multimeric complex along double-stranded RNA for efficient signal transduction. *Nat. Commun.* **2023**, *14*, 164. [CrossRef] [PubMed]

264. Kauffman, K.J.; Mir, F.F.; Jhunjhunwala, S.; Kaczmarek, J.C.; Hurtado, J.E.; Yang, J.H.; Webber, M.J.; Kowalski, P.S.; Heartlein, M.W.; DeRosa, F.; et al. Efficacy and immunogenicity of unmodified and pseudouridine-modified mRNA delivered systemically with lipid nanoparticles in vivo. *Biomaterials* **2016**, *109*, 78–87. [CrossRef] [PubMed]

265. Wadhwa, A.; Aljabbari, A.; Lokras, A.; Foged, C.; Thakur, A. Opportunities and Challenges in the Delivery of mRNA-based Vaccines. *Pharmaceutics* **2020**, *12*, 102. [CrossRef] [PubMed]

266. Uddin, M.N.; Roni, M.A. Challenges of Storage and Stability of mRNA-Based COVID-19 Vaccines. *Vaccines* **2021**, *9*, 1033. [CrossRef]

267. Leppek, K.; Byeon, G.W.; Kladwang, W.; Wayment-Steele, H.K.; Kerr, C.H.; Xu, A.F.; Kim, D.S.; Topkar, V.V.; Choe, C.; Rothschild, D.; et al. Combinatorial optimization of mRNA structure, stability, and translation for RNA-based therapeutics. *Nat. Commun.* **2022**, *13*, 1536. [CrossRef]

268. Chheda, U.; Pradeepan, S.; Esposito, E.; Strezsak, S.; Fernandez-Delgado, O.; Kranz, J. Factors Affecting Stability of RNA—Temperature, Length, Concentration, pH, and Buffering Species. *J. Pharm. Sci.* **2024**, *113*, 377–385. [CrossRef]

269. Kyuregyan, K.K.; Jansons, J.; Isaguliants, M. Is there a future for traditional immunogens when we have mRNA? *Microorganisms* **2023**, *11*, 1004. [CrossRef]

270. Bachmann, M.F.; Zeltins, A.; Kalnins, G.; Balke, I.; Fischer, N.; Rostaher, A.; Tars, K.; Favrot, C. Vaccination against IL-31 for the treatment of atopic dermatitis in dogs. *J. Allergy Clin. Immunol.* **2018**, *142*, 279–281.e1. [CrossRef]

271. Fettelschoss-Gabriel, A.; Fettelschoss, V.; Thoms, F.; Giese, C.; Daniel, M.; Olomski, F.; Kamarachev, J.; Birkmann, K.; Buhler, M.; Kummer, M. Treating insect-bite hypersensitivity in horses with active vaccination against IL-5. *J. Allergy Clin. Immunol.* **2018**, *142*, 1194–1205.e3. [CrossRef]

272. von Loga, I.S.; El-Turabi, A.; Jostins, L.; Miotla-Zarebska, J.; Mackay-Alderson, J.; Zeltins, A.; Parisi, I.; Bachmann, M.F.; Vincent, T.L. Active immunisation targeting nerve growth factor attenuates chronic pain behaviour in murine osteoarthritis. *Ann. Rheum. Dis.* **2019**, *78*, 672–675. [CrossRef] [PubMed]

273. Lu, S. Heterologous prime-boost vaccination. *Curr. Opin. Immunol.* **2009**, *21*, 346–351. [CrossRef] [PubMed]

274. Deming, M.E.; Lyke, K.E. A 'mix and match' approach to SARS-CoV-2 vaccination. *Nat. Med.* **2021**, *27*, 1510–1511. [CrossRef] [PubMed]

275. Jara, A.; Undurraga, E.A.; Zubizarreta, J.R.; González, C.; Pizarro, A.; Acevedo, J.; Leo, K.; Paredes, F.; Bralic, T.; Vergara, V.; et al. Effectiveness of homologous and heterologous booster doses for an inactivated SARS-CoV-2 vaccine: A large-scale prospective cohort study. *Lancet Glob. Health* **2022**, *10*, e798–e806. [CrossRef]

276. Vogt, A.-C.S.; Jörg, L.; Martina, B.; Krenger, P.S.; Chang, X.; Zeltins, A.; Vogel, M.; Mohsen, M.O.; Bachmann, M.F. Virus-Like Particles Are Efficient Tools for Boosting mRNA-Induced Antibodies. *Front. Immunol.* **2022**, *13*, 864718. [CrossRef]